学位論文
Doctor's Thesis

A fundamental study in the diagnosis of intracranial aneurysms with 3T MR angiography

(3T MR 血管撮影による脳動脈瘤診断の基礎的検討)

肥合　康弘

Yasuhiro Hiai

熊本大学大学院医学教育部博士課程病態制御学専攻放射線診断学

指 導 教 員

山下　康行　教授

熊本大学大学院医学教育部博士課程病態制御学専攻放射線診断学

2008 年 3 月

学 位 論 文

Doctor's Thesis

論文題名 ： A fundamental study in the diagnosis of intracranial aneurysms with 3T MR angiography

(3T MR 血管撮影による脳動脈瘤診断の基礎的検討)

著 者 名 ： 肥合 康弘
Yasuhiro Hiai

指導教員名： 熊本大学大学院医学教育部博士課程病態制御学専攻放射線診断学
山下 康行 教授

審査委員名： 形態構築学担当教授 児玉 公道
神経内科学担当教授 内野 誠
循環器病態学担当教授 小川 久雄
保健学教育部放射線技術科学担当教授 富口 静二

2008 年 3 月

Contents

Abstract

Background and Purpose:

Three-dimensional time-of-flight (3D TOF) MR angiography (MRA) is a noninvasive imaging modality and now readily accepted as a firstline diagnostic tool in MR examination of several cerebrovascular diseases. Concerning TOF MRA, the 3T system offers some potential advantages compared to 1.5T system. The various parameters of the 3D TOF MR angiograms such as the matrix size, reduction factor in parallel imaging, and acquisition time, however, have not been compared between 1.5T and 3T.

3D TOF MRA at 3T is feasible and useful in the follow up of patients with intracranial aneurysms treated with coil placement and the susceptibility-induced artifact created by platinum coils were minimal; however, they did not compare 3D TOF sequences between 1.5T and 3T.

The purpose of this study were two folds: (1) to analyze the influence of matrix, parallel imaging and acquisition time on image quality of 3D TOF MRA at 1.5T and 3T, and to illustrate whether the combination of larger matrices with parallel imaging technique is feasible, by evaluating the visualization of simulated intracranial aneurysms and aneurysmal blebs using a vascular phantom with pulsatile flow; and (2) to analyze the influence of the matrix and the echo time (TE) of 3D TOF MRA on the depiction of residual flow in aneurysms embolized with platinum coils at 1.5T and 3T and to establish the optimal parameters using a vascular

phantom with a pulsatile flow.

Materials and Methods:

An anthropomorphic vascular phantom was designed to simulate the various intracranial aneurysms, aneurysmal blebs and aneurysms embolized with platinum coils. The vascular phantom was connected to an electromagnetic flow pump with pulsatile flow, and we obtained 1.5 T and 3T MRAs altering the parameters of 3D TOF sequences including acquisition time. Two radiologists evaluated the depiction of the simulated aneurysms.

Results:

The aneurysmal blebs were not sufficiently visualized on the high-spatial-resolution 1.5T MRA (matrix size of 384 x 256 or 512 x 256) even with longer acquisition time (9 or 18 min.). At 3T with acquisition time of 4.5 min. using parallel imaging technique, however, the depiction of aneurysmal blebs was significantly better for the high-spatial-resolution sequence than for the standard resolution sequence. For the high-spatial-resolution sequence, the longer acquisition times did not improve the depiction of aneurysmal blebs in comparison with 4.5 minutes at 3T.

The increased spatial resolution and the shorter TE offered better image quality at 3T. For the depiction of an aneurysm remnant, the high-spatial-resolution 3T MRA (matrix size of 384×224 and 512 × 256)

with a short TE of 3.3 msec were superior to the 1.5T MRA obtained with any sequences.

Conclusion:

For 3D TOF MRA, the combination of the large matrix with parallel imaging technique is feasible at 3T, but not at 1.5T. 3T MRA is superior to 1.5T MRA for the assessment of aneurysms embolized with platinum coils.

Publication list

1. **Hiai Y**, Kakeda S, Sato T, Ohnari N, Moriya J, Kitajima M, Hirai T, Yamashita Y, Korogi Y.
3D TOF MRA of intracranial aneurysms at 1.5 T and 3 T: influence of matrix, parallel imaging, and acquisition time on image quality - a vascular phantom study. Acad Radiol. 2008; 15:635-640.

2. Kakeda S, Korogi Y, **Hiai Y**, Sato T, Ohnari N, Moriya J, Kamada K.
MRA of intracranial aneurysms embolized with platinum coils: a vascular phantom study at 1.5T and 3T. J Magn Reson Imaging. 2008; 28:13-20.

3. Goto T, Hamada K, Ito T, Nagao H, Takahashi T, Hayashida Y, **Hiai Y**, Yamashita Y.
Interactive scan control for kinematic study in open MRI.
Magn Reson Med Sci. 2007; 6:241-248.

4. Akter M, Hirai T, **Hiai Y**, Kitajima M, Komi M, Murakami R, Fukuoka H, Sasao A, Toya R, Haacke EM, Takahashi M, Hirano T, Kai Y, Morioka M, Hamasaki K, Kuratsu J, Yamashita Y.
Detection of hemorrhagic hypointense foci in the brain on susceptibility-weighted imaging clinical and phantom studies. Acad Radiol. 2007; 14: 1011-1019.

5. Hayashida Y, Hirai T, **Hiai Y**, Kitajima M, Imuta M, Murakami R, Nakayama Y, Awai K, Yamashita Y, Takahashi T, Hamada K.
Positional lumbar imaging using a positional device in a horizontally open-configuration MR unit - initial experience. J Magn Reson Imaging. 2007; 26: 525-528.

6. Kakeda S, Korogi Y, **Hiai Y**, Ohnari N, Moriya J, Kamada K, Hanamiya M, Sato T, Kitajima M.
Detection of brain metastasis at 3T: comparison among SE, IR-FSE and 3D-GRE sequences. Eur Radiol. 2007; 17: 2345-2351.

7. Nakayama Y, Li Q, Katsuragawa S, Ikeda R, **Hiai Y**, Awai K, Kusunoki S, Yamashita Y, Okajima H, Inomata Y, Doi K.
Automated hepatic volumetry for living related liver transplantation at multisection CT. Radiology. 2006; 240: 743-748.

8. Ikeda R, Katsuragawa S, Shimonobou T, **Hiai Y**, Hashida M, Awai K, Yamashita Y, Doi K.
Comparison of LCD and CRT monitors for detection of pulmonary nodules and interstitial lung diseases on digital chest radiographs by using receiver operating characteristic analysis. Nippon Hoshasen Gijutsu Gakkai Zasshi. 2006; 62: 734-741.

10. Liang L, Korogi Y, Sugahara T, Onomichi M, Shigematsu Y, Yang D, Kitajima M, **Hiai Y**, Takahashi M.
Evaluation of the intracranial dural sinuses with a 3D contrast-enhanced MP-RAGE sequence: prospective comparison with 2D-TOF MR venography and digital subtraction angiography. AJNR Am J Neuroradiol. 2001; 22: 481-492.

11. Mitsuzaki K, Yamashita Y, Sakaguchi T, Ogata I, Takahashi M, Hiai Y.
Abdomen, pelvis, and extremities: diagnostic accuracy of dynamic contrast-enhanced turbo MR angiography compared with conventional angiography-initial experience.
Radiology. 2000; 216:909-915.

12. Yamashita Y, Mitsuzaki K, Ogata I, Takahashi M, **Hiai Y**.
Three-dimensional high-resolution dynamic contrast-enhanced MR angiography of the pelvis and lower extremities with use of a phased array coil and subtraction: diagnostic accuracy. J Magn Reson Imaging. 1998; 8:1066-1072.

Acknowledgements

These academic investigations took place during my post graduate study period from 2004-2008, at the Department of Diagnostic Radiology, Graduate School of Medical Sciences, Kumamoto University and at the Department of Radiology, University of Occupational and Environmental Health.

I would like to express my sincere thanks to Professor Yasuyuki Yamashita, chairman of the department of Diagnostic Radiology, Graduate School of Medical Sciences, Kumamoto University, for his generous guidance and constructive instructions.

I am very grateful to Professor Yukunori Korogi, chairman of the Department of Radiology, University of Occupational and Environmental Health, School of Medicine, for his instruction of my research.

I would like to convey my sincere thanks to Dr. Toshinori Hirai, Associate Professor of the Department of Diagnostic Radiology, Graduate School of Medical Sciences, Kumamoto University, who instructed me during my research period.

I am also thankful to all other members of the Department of Diagnostic Radiology, Graduate School of Medical Sciences, Kumamoto University, for their kind supports.

Abbreviations

MRI: magnetic resonance imaging

MRA: magnetic resonance angiography

3D: three dimension

2D: two-dimensional

CE MRA: contrast enhanced MRA

DSA: digital subtraction angiography

TOF: time-of-flight

PC MRA: phase-contrast MRA

RF: radiofrequency

TR: repetition time

TE: echo time

VENC: velocity-encoding

SNR: signal to noise ratio

MOTSA: multiple overlapping thin slab acquisition

MT: magnetization transfer

TONE: tilted optimized nonsaturating excitation

3T: 3tesla

Chapter Ⅰ Background and Objectives

1. Introduction

2. Technical basics of magnetic resonance angiography (MRA)

1) Time-of- flight (TOF) MRA

2) Phase contrast (PC) MRA

3) Contrast-enhanced (CE) MRA

3. Application of TOF MRA for screening intracranial aneurysms

4. Factors affecting depiction of TOF MRA

5. Limitations of TOF MRA

6. Objectives

Chapter 1. Background and Objectives

1. Introduction

In conventional magnetic resonance imaging (MRI), the pulsatility of the blood flow usually causes artifacts. Signal intensities are often lower than expected from T1 or T2 values and the vessel cross sections may be visible a couple of times along the phase encoded direction. The understanding of these phenomena and the development of new techniques to counter these artifacts led, in the late 1980s, to the development of the so-called MR angiography (MRA) sequences. Signal intensities in the blood vessels became hyperintense and most artifacts were overcome. Two groups of sequences were developed in parallel and are still extensively used today: time-of-flight and phase contrast imaging. In the late 1990s, ultrafast acquisitions have been introduced for MRA. The availability of stronger gradients that can be switched on and off in an always shorter time, gave rise to three dimension (3D) techniques with extremely short TR. The short echo time makes the use of flow rephazing gradients obsolete. The T1 weighing is limited: only with a highly concentrated contrast agent in the vessels is a high signal intensity observed. In practice, contrast-enhanced (CE) MRA has to be performed during the first pass of the contrast bolus.

Technical advances in MRA have improved the accuracy of this technique in various clinical situations, such as aneurysms, arterial and venous steno-occlusive diseases, vascular malformations, inflammatory

arterial diseases, preoperative assessment of the patency of dural sinuses, and congenital vascular abnormalities. In many centers, MRA has replaced conventional digital subtraction angiography (DSA) in screening for intracranial vascular disease, because of its non-invasive and non-ionizing character.

2. Technical basics of MRA

Several MRA techniques have been developed for the imaging of the intracranial vascular system, such as time-of-flight MRA (TOF MRA), phase-contrast MRA (PC MRA), and more recently CE MRA.

1) TOF MRA

In TOF MRA, repetitive pulses are used to suppress stationary background tissues, while the unsuppressed protons of flowing blood create a signal. The high signal intensity in the blood vessels during TOF MRA is attributable to flow-related enhancement, and the absence of flow is characterized by reduced signal intensity (1). Hyperintense signal intensities in the blood vessel are not expected in T1-weighted acquisitions, since the T1 of the blood is not short. The paradoxical enhancement due to inflow phenomena in the TOF technique can be understood as follows: the spins in the blood vessel continuously enter (inflow) and leave the imaging volume. Therefore, they are subjected to a few radiofrequency excitation

pulses only, after which they are replaced by fresh blood. The surrounding tissues, on the other hand, are stationary and therefore are subjected to the complete series of radiofrequency (RF) pulses in an imaging sequence. The crucial fact is that in gradient echo acquisitions with small flip angles and short repetition time (TR). If the refreshment of the spins is not completed within one TR interval, the gradual signal decrease can be observed in the blood vessel.

The signal intensity changes during the series of RF pulses (Fig.1). After a first RF pulse, the signal intensity is large. After the second pulse, the signal intensity is already lower, and this effect continues until a (low) steady-state signal intensity is reached. In a 2D acquisition with, for example, a matrix of 256×512, the tissues in the imaging plane are subjected to 256 RF pulses. Stationary tissues experience all of them and

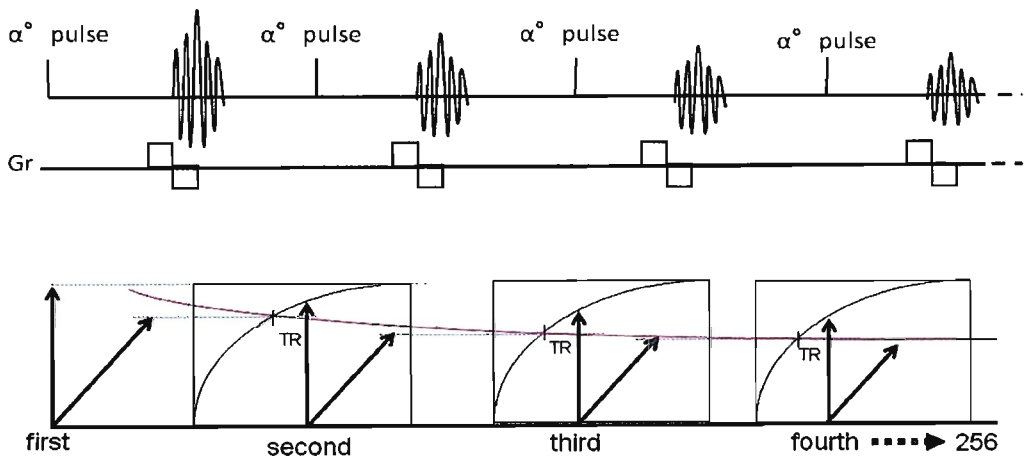

Figure 1. Gradient echo acquisitions with small flip angles(α) and short TR

their signal is therefore low. On the other hand, flowing spins that enter the slice experience only a few RF pulses and hence cause large signal intensities. The blood then leaves the imaging plane and is replaced by fresh blood that will experience again only a few pulses. Under these conditions, the hypo-intense steady-state value is never reached in the blood vessel.

2) PC MRA

PC MRA uses a different technique to create vascular contrast, based on manipulating the phase of the magnetization. This effect is obtained by applying a bipolar phase-encoding gradient and a velocity-encoding (VENC) factor (2, 3). Since PC MRA is sensitive to flow velocities, blood velocities higher than the preselected VENC value will not be represented or misrepresented in the image, so that the user must choose this value carefully. Higher VENC factors are necessary to image arteries selectively, whereas a VENC factor of 20 cm/s will represent the veins and sinuses(3) .

The one-to-one relation between the velocity of the spins and the phases they acquire when moving along a magnetic field gradient is the basis for phase contrast imaging. Whereas in TOF MRA flowing spins are optimally rephazed at the measurement, this is no longer the case in phase contrast imaging. The latter technique starts from a flow rephazed acquisition but adds additional bipolar gradient. (Fig.2)

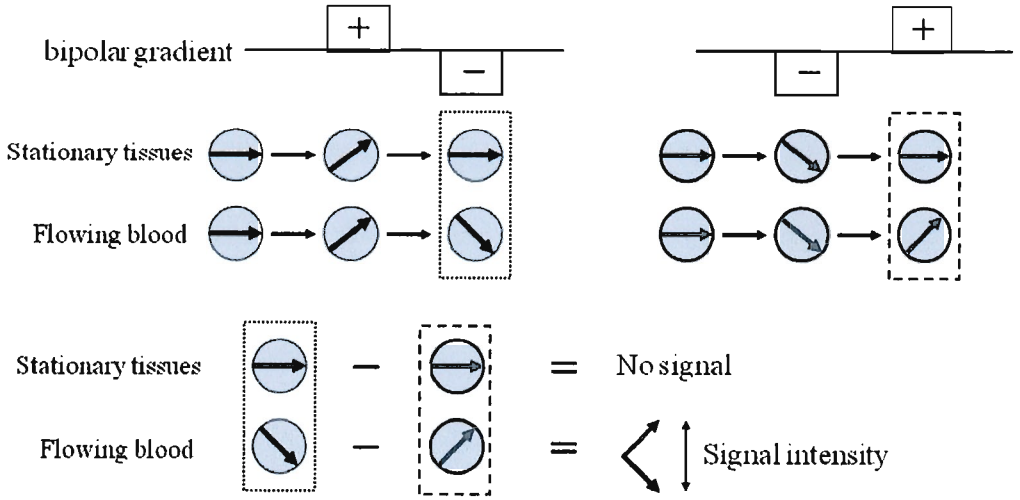

Figure 2. Phase Contrast (PC) MRA

These pulses have no effect on stationary spins, but leave spins that move along the direction of the gradients with a flow-induced phase that can be calculated. A phase contrast acquisition consists of minimally two measurements: a flow compensated (TOF) acquisition, and a second acquisition with bipolar gradient along a particular direction. After the subtraction of the corresponding phase images, flow along the direction of the bipolar gradient can be quantified (2). A complete flow picture is obtained for bipolar gradient along all three directions. The measurement takes rather long (four times longer than a corresponding TOF acquisition would take), but several optimizations are possible, due to the excellent vessel contrast (4).

Table. 1 Advantages, disadvantages and major applications of MRA

	advantages	disadvantages	major applications
3D TOF MRA	•No needs of contrast material •Less intravoxel dephasing •High SNR •Smoother vessel contour	•More saturation effects •Insensitive to slow flow •Artifacts attributable to thrombus and short T1 substances	•High-flow (arterial structures) •AVMs •Aneurysm •Carotid disease •screening
3D PC MRA	•No needs of contrast material •No saturation effects •Direction and quantification of flow velocities •Excellent background suppression	•Long acquisition time	•Cerebral arterie
3D CE MRA	•No saturation effects •Reduced intravoxel dephasing by gadolinium •High SNR •Excellent background suppression	•Venous puncture • High cost of gadolinium •Critical bolus timing and venous enhancement	•Cerebral arteries •Cerebral veins •Dynamic evaluation •of AVMs, •dural fistula, shunts •Aneurysm and treatment follow-up •Carotid disease

3) CE MRA

The MR signal on CE MRA depends on the T1 shortening effect of gadolinium. The intrinsic advantage of T1-based techniques is that they provide a morphological rather than a physiological image of the blood vessel. In theory, the appearance of the blood vessels is closer to the classical angiographic image than is the TOF or PC angiogram.

CE MRA has a higher signal to noise ratio (SNR) and a shorter acquisition time than other MRA techniques. However, the disadvantage of this technique is its imaging window, which is restricted to the first pass of the contrast bolus. CE MRA requires good coordination between the contrast injection, patient cooperation, and the starting time of the

acquisition. There are several methods to achieve proper bolus timing, such as simple fixed timing delay, test bolus, multiphase scanning, and real time fluoroscopic detection of contrast arrival (5).

3. Application of TOF MRA for screening intracranial aneurysms

DSA is still considered the gold standard in the investigation for intracranial aneurysms. False-negative rates of 5%-10% are reported in the literature, attributable not to limitations of spatial resolution, but to the limited number of projections of the neck of an aneurysm. Nevertheless, DSA requires a highly skilled radiologist to perform the procedure and remains an invasive technique with arterial puncture and intra-arterial catheter manipulation, with a 1% major complication risk and a 0.5% rate of persistent neurological deficit (6).

MRA, by its ability to obtain multiple projections, allows accurate evaluation of the anatomical implantation, the origin of the lesion, and the neck of the aneurysm. Technical advances in MRA throughout the 1990s have continued to improve the sensitivity of this technique for detecting cerebral aneurysms as a screening tool, and MRA has been used as an alternative to DSA for the presurgical work-up of aneurysmal subarachnoid hemorrhage (7). Aneurysms as small as 3 mm can now be detected with 3D TOF MRA (8). Once obtained, MRA data can be viewed from any projection in both 2D and 3D reformation algorithms to detect the aneurysm and to evaluate its neck. Multiplanar reformations are

particularly helpful in defining the neck and also the parent and branch vessels related to aneurysms (9). The detection and treatment of an aneurysm before it ruptures with possible lethal subarachnoid hemorrhage is an important research topic. TOF MRA can identify aneurysms (at least 3 mm in size) with a sensitivity of 74%-98% (8, 10). MRA is ideal for screening cerebral aneurysms because the procedure is noninvasive and the patient is not exposed to radiation.

The role of endovascular treatment in the management of patients with intracranial aneurysms is increasing. Indications for endovascular occlusion with coils and minimization of the risks of thromboembolic complications depend on a number of factors, such as the analysis of the neck/fundus ratio and the understanding of the relationship of the aneurysm to both parent and branch vessels (11). If a residual aneurysm or aneurysm regrowth is identified, retreatment is often considered (12). This routine follow-up is usually made with DSA. However, a few studies with 3D TOF MRA have reported the potential role of MRA in the follow-up, with sensitivity rates ranging from 71% to 91% and the specificity rates ranging from 89% to 100% in ruling out residual flow (12, 15). False-negative examinations can be explained by the presence of slow flow in the aneurysm with a saturation phenomenon or magnetic susceptibility artifact of the coil mass (12.15). False-positive examinations are probably related to blood clot(s) within the coil mass, which can be interpreted as flow (12).

Thus, in the screening of intracranial aneurysms, 3D TOF MRA is now the most widely used sequence.

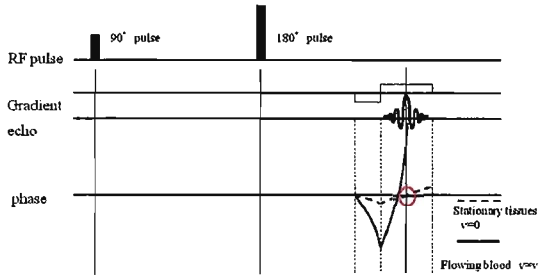

Figure 3(a). Flow compensation

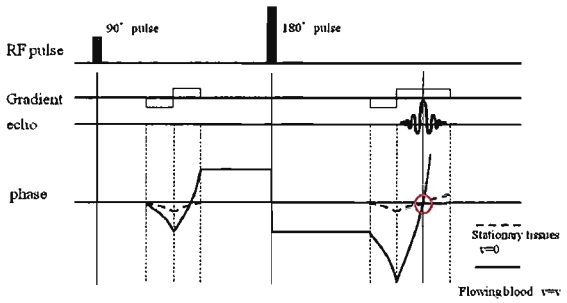

Figure 3(b). Flow compensation

4. Factors affecting depiction of TOF MRA

The hyperintense signal intensities in the TOF are derived from inflow effects. The basic sequence is a gradient recalled echo technique with short TR: echo time (TE), enabling the acquisition of two-dimensional (2D) or 3D images in a reasonable time period. The artifacts along the phase encoded direction are overcome by using dedicated gradient schemes ('gradient motion refocusing gradients' or 'first order flow compensating gradients'). The result is a poorly T1-weighted measurement. The understanding of the flow-induced effects along the phase encoded direction and the proposition of dedicated schemes to compensate for these effects were a necessary step for the introduction of the 'TOF' technique (16, 17). Mispositioning along the phase encoded direction has been explained by the phase behavior of moving spins: gradient refocusing schemes, such as routinely used to make gradient and spin echoes, fail to provide in phase signals for spins that move along the direction of the

gradient. (Figure 3(a)) Gradient motion rephazing consists of replacing any couple of balanced pulses by three pulses. These schemes ensure in phase signals for spins that flow with a constant velocity. In practice it means that the signal intensity is not increased, but that signal voids or ghost signals are largely eliminated. The vessel can be visualized with the signal as predicted by the inflow effect. (Figure 3(b)) As a result, the hyperintense signal intensities in the blood vessels depend not only on the inflow effect, but also on the type of flow. Only with laminar flow do the special flow rephazing gradients perform properly. Spin rephazing in case of turbulent flow remains unpredictable.

In practice, the applicability of the technique depends on the velocity of the blood in the vessel, the length of the vessel in the imaging slab, the flow pattern and the sequence parameter setting. Whenever the blood remains for a longer period in the slice or slab, the signal becomes saturated. It is particularly difficult to visualize veins and slow flowing arterial blood in patients with low cardiac output, in obstructive diseases or in highly resistant vessels. Other determining factors are artifacts due to respiratory motion or intrinsic organ motion.

Image quality on 3D TOF MRA can be improved by use of a technique called "multiple overlapping thin slab acquisition (MOTSA)"

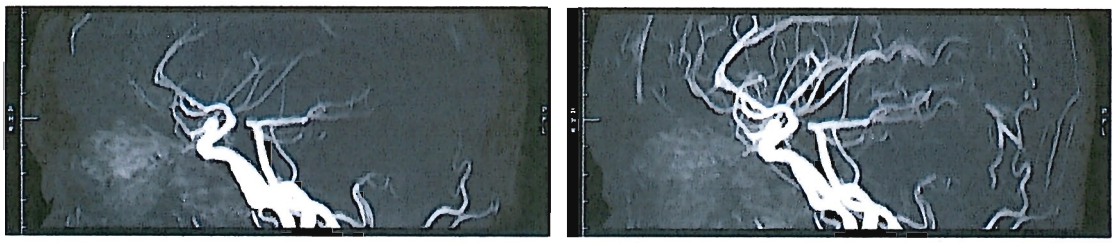

Single slab
1'10"

MOTSA
1'50"

Figure 4. Multiple Overlapping Thin Slab Acquisition(MOTSA)

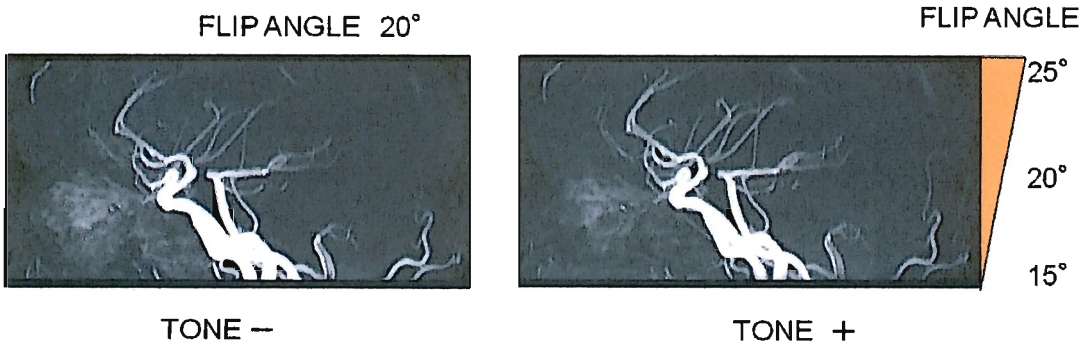

Figure 5. Tilted Optimized Nonsaturating Excitation(TONE)

(Fig. 4), to overcome flow saturation effects, and by the application of magnetization transfer (MT) prepulses to suppress the background signal of the stationary tissues (18, 19). Saturation effects can also be minimized by using lower flip angles (15-20) in combination with longer TRs, thiner slices, and the shortest possible TE (20). The variable flip-angle excitation technique, termed "tilted optimized nonsaturating excitation (TONE) " (fig. 5), has also been shown to increase the signal and lower the

spin phase dispersion effect within the vessels (21). In this technique, the flip angle varies across the slab that it is set lower at the inlet side and gradually increases as it approaches the exit side to increase the blood signal (21).

The remaining saturation effects of slow-flow in small arterial branches can be further eliminated by intravenous injection of paramagnetic contrast material, but with the disadvantages of increased cost, possible superimposition of veins, and enhancement of surrounding tissues (22).

5. Limitations of TOF MRA

The main limitations of the technique are the spin dephasing that occurs in complex or turbulent flow pattern, particularly in 3D TOF, and in vessels in close proximity to tissues with short T1, such as fat or subacute hemorrhage. Signal loss may also occur in the presence of flow resulting from the spin saturation effect, as in the case of slow flow in the distal intracranial vessels, or becuase of intravoxel phase dispersion, as in situations of turbulent flow or magnetic field inhomogeneities (1, 23). The TOF technique shows the intracranial aneurysm but the signal intensity is reduced due to slow or turbulent flow in the aneurysmal sac.

Disadvantages of MRA are reduced visualisation of very small distal cortical or deep branches, poor temporal information, poor selectivity and dependence on flow or patient's cooperation. Here we will limit ourself to a summary of some essential elements. The high quality of intracranial MRA

is based on the substantial inflow effect throughout the cardiac cycle, the small volume of interest and the minimal effects of the most common causes of MR artifacts, such as respiration, cardiac motion, and susceptibility changes on the head. Any material whose static magnetic susceptibility differs from that of surrounding tissues will distort the magnetic (B0) field. In addition, dynamic eddy currents in the conduction of materials caused by time variable magnetic fields, such as RF and B0 gradient fields, may lead to B1 field homogeneity, image intensity, and distortion artifacts (24). These effects with metal also cause the image degradation in 3D TOF MRA, which is the limiting factor in the assessment of aneurysm remnants and parent vessel stenosis after aneurysm coiling (25).

6. Objectives

With regard to 3D TOF MRA, the 3T system offers some potential advantages compared to a 1.5T system. The approximate doubling of the SNR from 1.5 to 3T can provide higher spatial resolution (26, 27) and the increased T1 relaxation time at higher magnetic field strength yields improvement of vessel-tissue contrast at 3T imaging (28). Therefore, these advantages provide prospects for further improvement of depiction of aneurysm. The various parameters of the 3D TOF MRA such as the matrix size, reduction factor in parallel imaging, acquisition time and TE, however, have not been compared between 1.5T and 3T. On the other hand, one of

the major limitations of 3T MRA is its greater susceptibility effects, which can increase the varying degrees of susceptibility-induced artifact created by embolized platinum coils.

The purpose of this study is to analyze the influence of matrix, parallel imaging, acquisition time and TE on image quality of 3D TOF MRA at 1.5T and 3T, and to illustrate whether the combination of larger matrices with parallel imaging technique is feasible, by evaluating the visualization of simulated intracranial aneurysms and residual flow in aneurysms embolized with platinum coils using a vascular phantom with pulsatile flow.

Chapter Ⅱ 3D TOF MRA of intracranial aneurysms at 1.5T and 3T: Influence of matrix, parallel imaging and acquisition time on image quality --A vascular phantom study

1. Abstract
2. Introduction
3. Materials and Methods
4. Results
5. Discussion

1.Abstract

Purpose:

A 3T MRI system provides a better signal-to-noise ratio and inflow effect than 1.5T in 3D TOF MRA. The purpose of this study is to analyze the influence of matrix, parallel imaging and acquisition time on image quality of 3D TOF MRA at 1.5T and 3T, and to illustrate whether the combination of larger matrices with parallel imaging technique is feasible, by evaluating the visualization of simulated intracranial aneurysms and aneurysmal blebs using a vascular phantom with pulsatile flow.

Materials and Methods:

An anthropomorphic vascular phantom was designed to simulate the various intracranial aneurysms with aneurysmal bleb. The vascular phantom was connected to an electromagnetic flow pump with pulsatile flow, and we obtained 1.5 T and 3T MRAs altering the parameters of 3D TOF sequences including acquisition time. Two radiologists evaluated the depiction of simulated aneurysms and aneurysmal blebs.

Results:

The aneurysmal blebs were not sufficiently visualized on the high-spatial-resolution 1.5T MRA (matrix size of 384 x 256 or 512 x 256) even with longer acquisition time (9 or 18 min.). At 3T with acquisition time of 4.5 min. using parallel imaging technique, however, the depiction of aneurysmal blebs was significantly better for the high-spatial-resolution sequence than for the standard resolution sequence. For the high-spatial-resolution sequence, the longer acquisition times did not

improve the depiction of aneurysmal blebs in comparison with 4.5 minutes at 3T.

Conclusion:

For 3D TOF MRA, the combination of the large matrix with parallel imaging technique is feasible at 3T, but not at 1.5T.

2.Introduction

Three-dimensional time-of-flight (3D TOF) MR angiography (MRA) is a noninvasive imaging modality and now readily accepted as a firstline diagnostic tool in MR examination of several cerebrovascular diseases (29-32). Concerning TOF MRA, the 3T system offers some potential advantages compared to 1.5T system. The approximate doubling of signal-to-noise ratio from 1.5 to 3T can provide the higher spatial resolution (33, 34) and the increased T1 relaxation time at higher magnetic field strength yields improvement of vessel-tissue contrast at 3T imaging (28). Several previous studies have reported that the high-spatial-resolution 3T MRA allowed better visualization of small vessel segments and vascular disease, including intracranial aneurysms and intracranial stenoses and obstructions (33, 34, 35, 36). The various parameters of the 3D TOF MR angiograms such as the matrix size, reduction factor in parallel imaging, and acquisition time, however, have not been compared between 1.5T and 3T.

The purpose of this study is to analyze the influence of matrix, parallel imaging and acquisition time on image quality of 3D TOF MRA at

1.5T and 3T, and to illustrate whether the combination of larger matrices with parallel imaging technique is feasible, by evaluating the visualization of simulated intracranial aneurysms and aneurysmal blebs using a vascular phantom with pulsatile flow.

3.Materials and Methods

Phantom Design

An anthropomorphic vascular phantom (Renaissance of Technology Corporation, Shizuoka, Japan) consisted of a 19-cm-diameter cylinder made of silicone rubber was designed to simulate the bilateral intracranial arteries with various intracranial aneurysms. Two types of simulated aneurysms - 17 aneurysms with diameter of 3 mm and 15 aneurysms with diameter of 6 mm - were placed on the simulated internal carotid artery, anterior cerebral artery and middle cerebral artery (Figure 1). Of all 32

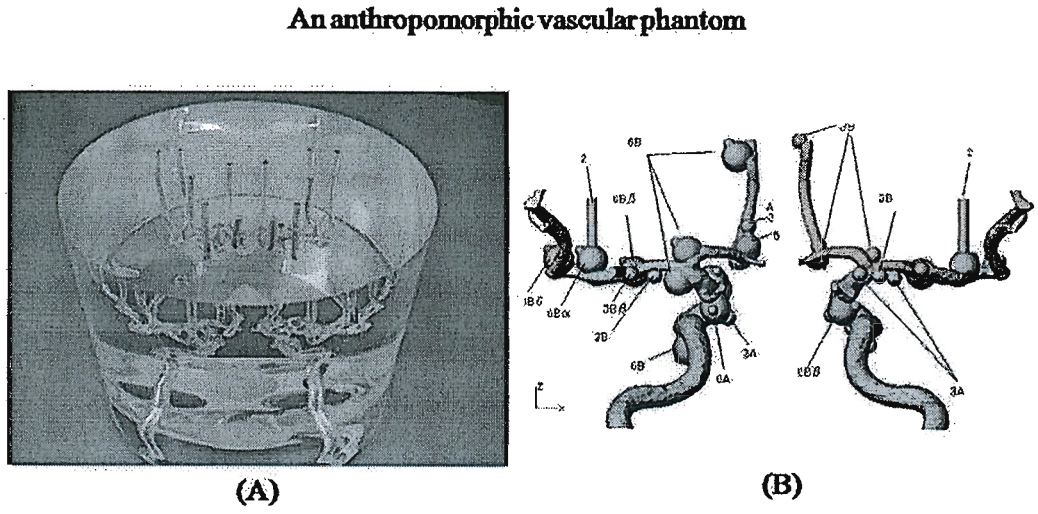

Figure 1, A and B. Photograph (A) and schematic drawing (B) of the anthropomorphic vascular phantom used in this study. The phantom was designed to simulate the intracranial arteries with a total of 32 aneurysms. Of 32 aneurysms, 15 had an aneurysmal bleb with diameter of 2 mm.

aneurysms, 15 had an aneurysmal bleb with diameter of 2 mm, which was placed at a tip onto the surface of the aneurysm.

Image Acquisition

The phantom tube filled with gadodiamide-saline solution was connected to an electromagnetic flow pump (LMI Milton Roy, Acton, MA) that allowed pulsatile perfusion with pulse rates between 40 and 100 beats per minute. The phantom was connected to a system of reservoirs and a pump that maintained a constant pressure difference across the flow tube within the phantom. Pulsatile flow was generated by a pulsatile blood pump (model 1405; Harvard Apparatus An Ealing; South Natick, Mass). In this pump, an electric motor drives a flywheel, which pushes a plunger in and out of a cylinder. As the plunger moves forward, flow is ejected out of the one-way valve and is propelled toward the flow circuit. Pulsatile flow with a pulsation rate of 50 pulses per minute and mean velocity of 25cm/sec (maximum; 50 cm/sec) was produced in the experimental assembly in a closed system. To emulate the characteristics of blood, the T1 of the solution obtained at 1.5T was adjusted to approximately 900 msec with gadopentetate dimeglumine (41), and all examinations at 1.5T and 3T were obtained by using this solution.

MR angiographic studies were obtained with a Signa EXCITE 1.5T MR system (GE Medical Systems, Milwaukee, Wis) and a Signa EXCITE 3T MR system (GE Medical Systems, Milwaukee, Wis) by using a dedicated eight-channel phased-array coil (USA Instruments Aurora, Ohio).

Table 1, Scanning parameters for the 3D time-of-flight MR angiography and results in evaluation for the depiction of simulated lesions.

Sequence No.	TR	TE	FA	BW	FOV	F-E mtx	ST	RF	NEX	AT	Mean score for image quality (mean ± standard error) Aneurysm	Bleb
1.5T												
1	30	6.3	20	31.25	180 mm	128x128	1.0 mm	2	1 time	2 min 18 sec	3.10±0.51	2.20±1.095
2	30	6.3	20	31.25	180 mm	192x192	1.0 mm	2	1 time	3 min 25 sec	3.00±0.42	2.00±1.000
3	30	6.3	20	31.25	180 mm	256x256	1.0 mm	2	1 time	4 min 32 sec	2.58±0.51	1.20±0.447
4	30	6.3	20	31.25	180 mm	256x256	1.0 mm	1.3	1 time	6 min 47 sec	3.30±0.77	2.80±0.837
5	30	6.3	20	31.25	180 mm	256x256	1.0 mm	NA	1 time	9 min 1 sec	3.89±0.79	4.00±1.000
6	30	6.3	20	31.25	180 mm	256x256	1.0 mm	NA	2times	17 min 59 sec	4.08±0.66	4.20±0.837
7	30	6.3	20	31.25	180 mm	384x256	1.0 mm	2	1 time	4 min 32 sec	2.25±0.75	1.00±0.000
8	30	6.3	20	31.25	180 mm	384x256	1.0 mm	1.3	1 time	6 min 47 sec	3.20±0.71	1.80±1.095
9	30	6.3	20	31.25	180 mm	384x256	1.0 mm	NA	1 time	9 min 1 sec	3.17±0.49	2.20±0.837
10	30	6.3	20	31.25	180 mm	384x256	1.0 mm	NA	2times	17 min 59 sec	3.70±0.49	3.40±0.548
11	30	6.3	20	31.25	180 mm	512x256	1.0 mm	2	1 time	4 min 32sec	2.08±0.66	1.00±0.000
12	30	6.3	20	31.25	180 mm	512x256	1.0 mm	NA	2time	17 min 59 sec	3.80±0.38	2.80±0.447
3T												
1	30	6.3	20	31.25	180 mm	128x128	1.0 mm	2	1 time	2 min 18 sec	3.60±0.51	3.25±0.837
2	30	6.3	20	31.25	180 mm	192x192	1.0 mm	2	1 time	3 min 25 sec	3.70±0.45	3.40±0.548
3	30	6.3	20	31.25	180 mm	256x256	1.0 mm	2	1 time	4 min 32 sec	4.00±0.73	4.20±0.837
4	30	6.3	20	31.25	180 mm	384x256	1.0 mm	2	1 time	4 min 32 sec	4.40±0.51	4.20±0.837
5	30	6.3	20	31.25	180 mm	384x256	1.0 mm	1.3	1 time	7 min 16 sec	4.80±0.38	4.40±0.894
6	30	6.3	20	31.25	180 mm	384x256	1.0 mm	NA	1 time	9 min 1 sec	4.80±0.38	4.60±0.894
7	30	6.3	20	31.25	180 mm	512x256	1.0 mm	2	1 time	4 min 32 sec	4.80±0.38	4.40±0.548

Note.—TR, repetition time; TE, echo time; FA, flip angle; BW, bandwidth; FOV, field of view; F-E mtx, frequency-encoded matrix; ST, section thickness; RF, reduction factor; NEX, number of excitation; AT, acquisition time; NA, not applicable

The various 3D TOF sequences were performed at 1.5 T and 3T MRI systems (Table 1). For all 3D TOF sequences, the variables included the matrix size, reduction factor in parallel imaging, and acquisition time. The following parameters were kept constant: repetition time (TR), echo time (TE), bandwidth (BW), field of view (FOV), flip angle, and section thickness.

Image Analysis of MRA

A certified neuroradiologist (S.K.) interpreted the MR angiograms, and selected the 12 simulated aneurysms (with bleb; 5, without bleb; 7) for the evaluation; the aneurysms containing air bubbles in the phantom lumen were eliminated in this process. For the image quality of the MRA obtained from various sequences with 1.5T and 3T systems, two

neuroradiologists (N.Oh, J.M.) independently evaluated the reproducibility of MR angiograms in the assessment of simulated aneurysms and aneurysmal blebs. For interpretation of MRA, these radiologists were blinded to the MR imaging systems (1.5T and 3T systems) and MR imaging parameters (TE, voxel dimension, acquisition time, etc.). The volume-rendered (VR) display was used for this evaluation of MR angiograms. In assessing the MR angiograms, each image was analyzed separately and only one image was shown at a time. After independent interpretations were performed, the differences in assessment of both observers were resolved by consensus. The schematic drawing of an anthropomorphic vascular phantom was always used as the standard of reference (Fig 1. B), and the radiologists rated the aneurysm and aneurysmal bleb depiction using a 5-point scale as follows; 5=excellent (an aneurysm or aneurysmal bleb was depicted with same quality, which is close to that at the schematic drawing), 4=more than adequate (aneurysm or aneurysmal bleb was clearly depicted but image quality somewhat reduced compared with that at the schematic drawing), 3=adequate (depiction of the aneurysm or aneurysmal bleb was still sufficient), 2 = insufficient visualization, 1 = not visible.

The MR angiograms were displayed and interpreted on a diagnostic monitor (Flexscan L365; EIZO NANAO, Ishikawa, Japan). An intuitive and efficient user interface allows the manipulation of these views in real time, and the reviewers determined the threshold of vessel images in each subject by interactively observing the angiograms at the workstation.

Statistical Analysis

For evaluation, statistical analyses were performed with a statistical software package (StatView 5.0; SAS Institute, Cary, NC). For the scores of overall image quality, all results were expressed as the mean ± standard error of the mean for each sequence obtained with both field strengths. Analysis of Wilcoxon signed rank test was performed on the results to assess the statistical significance of the different scores assigned to the each sequence. A P value of less than 0.05 was considered to indicate a statistically significant difference. To evaluate the level of interobserver agreement of scores of image quality for the aneurysms and aneurysmal blebs, a Kendall W test was performed. Kendall W coefficients between 0.5 and 0.8 were considered to indicate good agreement, and coefficients higher than 0.8 were considered to indicate excellent agreement.

4.Results

For the depiction of the simulated aneurysm and aneurysmal bleb on 1.5T and 3T MR angiograms, results of the final consensus reviewed by two radiologists are summarized in Table 1.

Relationship between matrix size and image quality of MR angiograms with use of parallel imaging (reduction factor=2)

The radiologists scored the depiction of simulated aneurysms and aneurysmal blebs as "excellent (score 5)" or "more than adequate (score

4)" on all higher spatial-resolution 3T MR angiograms (mean image score = 4.20 with matrix size of 384 x 256 and 4.40 with matrix size of 512 x 256). At 3T, the average reader ratings regarding the depiction of aneurysmal blebs were significantly higher for the higher spatial-resolution sequence than for the standard resolution sequence (mean image score: 4.20 with matrix size of 384 x 256 versus 3.40 with matrix size of 192 x 192, p=0.016) (Figures 2 and 3). At 1.5T, however, the aneurysmal blebs were not sufficiently visualized with the matrix size of 384 x 256 and 512 x 256, and the overall image quality were scored as "not visible (score 1)" (Figures 2 and 3).

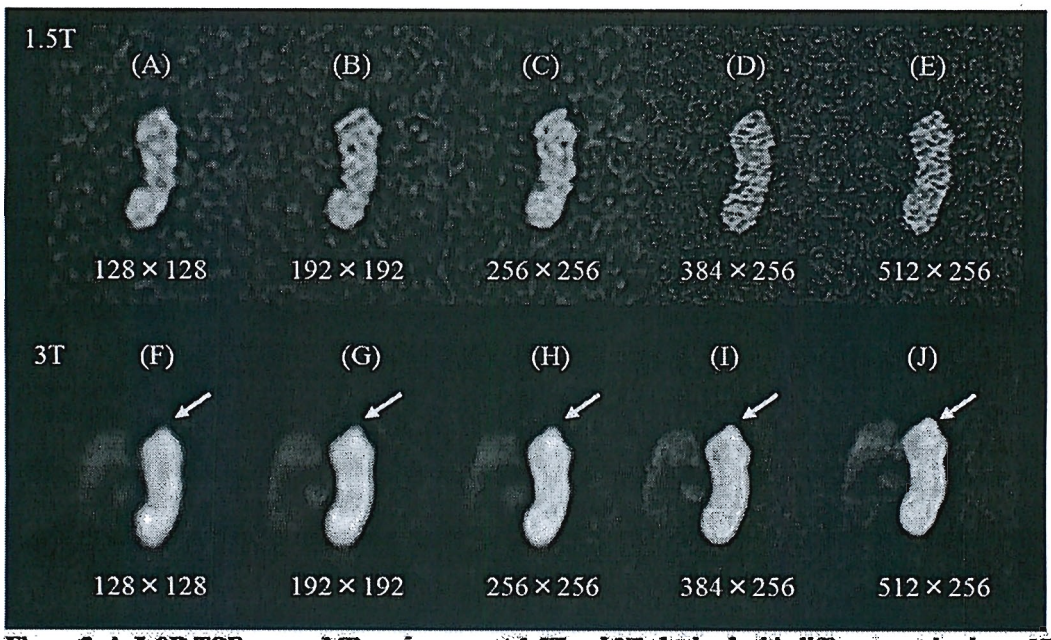

Figure 2, A-J. 3D TOF source MR angiograms at 1.5T and 3T obtained with different matrix sizes. 3D TOF source MR angiogram at 1.5T with a matrix size of 128x128 (A), 192x192 (B), 256x256 (C), 384x256 (D), and 512x256 (E). 3D TOF source MR angiogram at 3T with a matrix size of 128x128 (F), 192x192 (G), 256x256 (H), 384x256 (I), and 512x256 (J). On source MR angiograms at 1.5T, a higher matrix size leads to signal loss in vessel lumen. At 3T, the image quality regarding the depiction of an aneurysmal blebs is gradually superior as the matrix size increases (arrows).

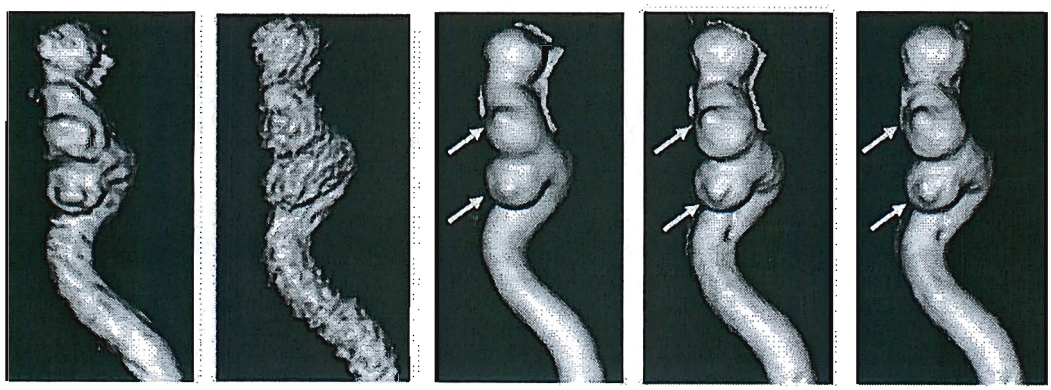

Figure 3, A-E. 3D TOF MR angiograms at 3T and 1.5T obtained with various matrix size using reduction factor of two. 3D TOF VR anterior projection at 1.5T with a matrix size of 192x192 (A) and 384x256 (B). 3D TOF VR anterior projection at 3T with a matrix size of 192x192 (C), 384x256 (D), and 512x256 (E). The aneurysmal blebs were not visualized on the 1.5T MR angiogram with the matrix size of 384 x 256 (B), and the MR angiogram with the matrix size of 192 x 192 (A) was scored as "insufficient visualization". On 3D TOF MR angiograms at 3T (C-E), the image quality regarding the depiction of aneurysmal blebs was gradually superior as the matrix size increases (arrows).

Relationship between acquisition time (reduction factor) and image quality of MR angiograms

Figure 4 shows the comparison of the average reader ratings regarding the depiction of aneurysmal blebs at 1.5T and 3T MRA obtained with various acquisition times (reduction factors). The image degradation increased with increased reduction factor at 1.5T. For example, with the matrix size of 256 x 256, the reduction factor of 2 showed a significant degradation of image quality (mean image score = 1.20) compared with the reduction factor of 1 (mean image score = 4.00, $p<0.01$) and 1.3 (mean image score = 2.80, $p=0.034$) (Figure 5). At 3T, however, the image quality was not influenced by the reduction factor with the matrix of 384 x 256 (Figure 5); that is, the longer acquisition times (7 min. or longer) did not necessarily improve the depiction of aneurysmal blebs.

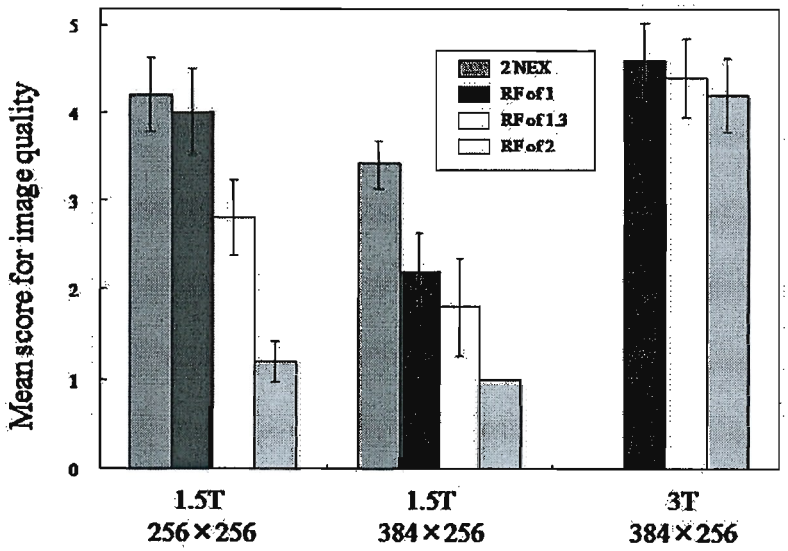

Figure 4. Comparison of the average reader ratings regarding the depiction of aneurysmal blebs at 1.5T and 3T obtained with various acquisition times (reduction factors). With the matrix size of 256 x 256 or 384×256 at 1.5T, the reduction factor of 2 shows a degradation of image quality compared with the reduction factor of 1 (no use of parallel imaging) and 1.3. The image quality of 3T MRA with the matrix size of 384×256 is not influenced by the reduction factor.

The aneurysmal blebs were not sufficiently visualized on the higher spatial-resolution 1.5T MRA (matrix size of 384 x 256 or 512 x 256) even with longer acquisition time (9 min. or 18 min.). At 1.5T, best image quality was obtained with the matrix of 256 x 256. When 1.5T with the matrix of 256 x 256 and 3T with the matrix of 384 x 256 were compared, the 3T MRA with the acquisition time of 4.5 minutes (mean image score = 4.20) was superior to 1.5T MRA with the acquisition time of 9 minutes (mean image score = 4.00) and almost equivalent to the 1.5T MRA with an acquisition time of 18 minutes (mean image score = 4.20) (Figure 6).

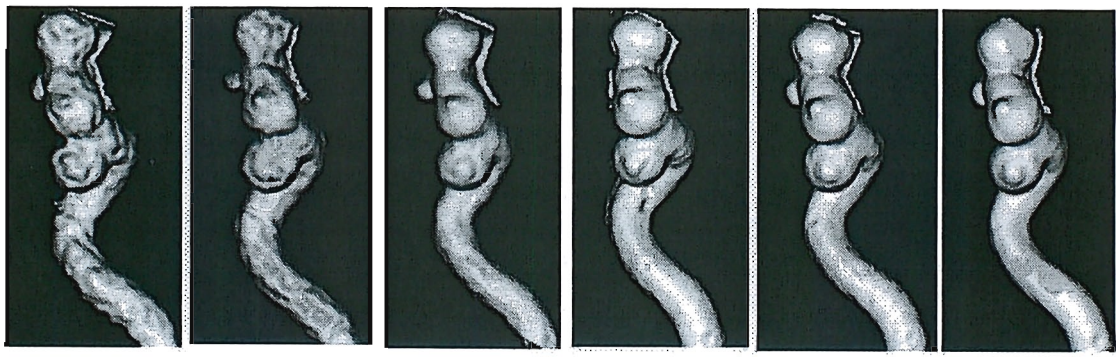

Figure 5, A-F. 3D TOF MR angiograms at 1.5T (matrix size of 256 x 256) and 3T (matrix size of 384 x 256) obtained with various reduction factors. 3D TOF VR anterior projection at 1.5T with the use of a reduction factor of two (A), 1.3 (B), and one (not applicable) (C). 3D TOF VR anterior projection at 3T with the use of a reduction factor of two (D), 1.25 (E), and one (not applicable) (F). Although the image quality of 3T MRA was not influenced by the reduction factor (D-F), the image quality at 1.5T was degraded as increasing reduction factor (A-C).

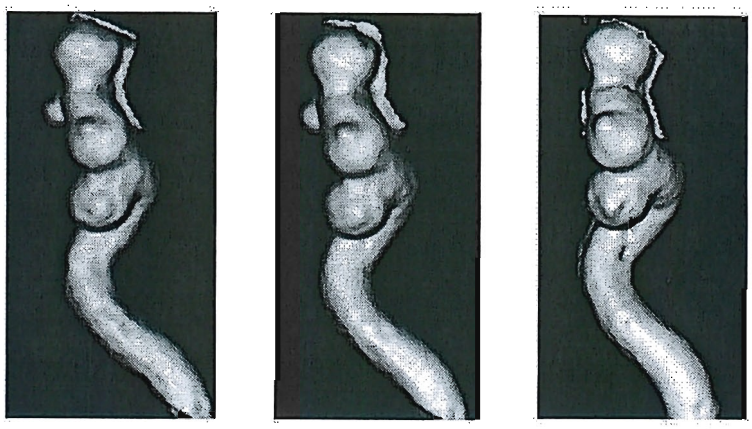

Figure 6, A-C. 3D TOF MR angiography at 1.5T (matrix size of 256 x 256) obtained with an acquisition time of 9.1 minutes (A) and 17.59 minutes (two signals acquired; NEX=2) (B), and 3T (matrix size of 384 x 256, reduction factor of two) obtained with an acquisition time of 4.32 minutes. Regarding the depiction of aneurysmal blebs, 3T MR angiogram with an acquisition time of 4.32 minutes (C) was superior to 1.5T MR angiogram with an acquisition time of 9.1 minutes (A), and almost equivalent to 1.5T MR angiogram with an acquisition time of 17.59 minutes (B).

Interobserver Agreement

For evaluation of MR angiograms, interobserver agreement between the two radiologists in rating the depiction of aneurysms and aneurysmal blebs was good for both the 3T system and the 1.5T system; with Kendall *W* values (τ), 0.51 vs 0.55 for aneurysms, and 0.52 vs 0.63 for aneurysmal blebs, respectively.

5.Discussion

Winfried et al have reported that the high-spatial-resolution 3D TOF MRA at 3T is superior to that at 1.5 T in the diagnosis of cerebrovascular disease (33). Similar to previous assertions, our results of 3T MRA demonstrated that the depiction of simulated aneurysms and aneurysmal blebs was gradually superior as matrix size increased. With the improved signal-to-noise ratio at 3T, it is possible to increase spatial resolution at 3D TOF MRA with preservation of image quality (33, 34). In contrast, the simulated aneurysmal blebs were not sufficiently visualized on high-spatial-resolution 1.5T MRA. Further increases in spatial resolution cause further reduction of signal-to-noise ratio, and this would result in the image degradation at 1.5T MRA regarding the depiction of aneurysms and aneurysmal blebs. Therefore, the spatial resolution at 3D TOF MRA may be still limited at 1.5T, even if longer acquisition times are used.

The parallel imaging techniques such as array spatial sensitivity encoding technique (ASSET) and sensitivity encoding (SENSE) has been

proposed to markedly reduce image acquisition time (38-40); however, the decrease in signal-to-noise ratio inherent to parallel imaging technique also has been reported (39). According to the experimental data (39-42), the reduction in signal-to-noise ratio is characterized by the square root of the reduction factor. Gaa J et al. have reported that the parallel imaging technique is more beneficial for 3T MRA than for 1.5T MRA, because the higher SNR available at 3T allows for higher spatial resolution without prolongation of measurement time (36). Similar to this previous assertion, our study also showed that the parallel imaging technique did not degrade the MRA image at 3T, but at 1.5T. The high-spatial resolution 3T MRA may certainly benefit from the use of parallel imaging technique to reduce the acquisition time while maintaining the high spatial resolution. In this study, the 3T MRA with an acquisition time of 4.5 minutes using parallel imaging technique provided a high-quality imaging for the depiction of aneurysmal blebs. Moreover, among 3T MRAs obtained with acquisition times more than 4.5 minutes, there were no significant differences for the average reader ratings in the depiction of aneurysmal blebs. For the 3D TOF MRA at 3T, therefore, an acquisition time of 4.5 minutes using parallel imaging technique seems clinically feasible; the longer acquisition times may be associated with poor image quality because of the increasing risk of patient movements.

Our study has some limitations. First, we used the anthropomorphic vascular phantom, because, in a clinical study, it is impossible to compare the visualization of aneurysms using the various parameters between 1.5T

and 3T MRA. Although vascular phantom studies cannot always simulate clinical conditions, we still believe that our data provided important information about the influence of matrix, parallel imaging and acquisition time on the image quality and the clinical settings of MRA sequences at 3T. Second, although the MIP technique is most widely applied for the postprocessing of 3D TOF MRA, we used the volume-rendering (VR) technique as the only 3D display method, which maintains the original anatomic spatial relationships of the 3D data set, for evaluating the MR angiograms. Our study did not aim to compare the detectability of the simulated intracranial aneurysms, but to compare the visualization, especially of aneurysmal blebs.

In conclusion, for 3D TOF MRA, the combination of the large matrix with parallel imaging technique is feasible at 3T, but not at 1.5T. The 3T system allowed shorter acquisition time less than 5 minutes with the use of parallel imaging technique while maintaining the higher spatial resolution.

Chapter Ⅲ MRA of Intracranial Aneurysms Embolized With Platinum Coils: A Vascular Phantom Study at 1.5T and 3T

1. Abstract
2. Introduction
3. Materials and Methods
4. Results
5. Discussion

1. Abstract

Purpose: To analyze the influence of matrix and echo time (TE) of three-dimensional time-of-flight (3D TOF) magnetic resonance angiography (MRA) on the depiction of residual flow in aneurysms embolized with platinum coils at 1.5T and 3T.

Materials and Methods: A simulated intracranial aneurysm of the vascular phantom was loosely packed to maintain the patency of some residual aneurysmal lumen with platinum coils and connected to an electromagnetic flow pump with pulsatile flow. MRAs were obtained altering the matrix and TE of 3D TOF sequences at 1.5T and 3T.

Results: The increased spatial resolution and the shorter TE offered better image quality at 3T. For the depiction of an aneurysm remnant, the high-spatial-resolution 3T MRA (matrix size of 384×224 and 512 × 256) with a short TE of 3.3 msec were superior to the 1.5T MRA obtained with any sequences.

Conclusion: 3T MRA is superior to 1.5T MRA for the assessment of aneurysms embolized with platinum coils; the combination of the 512×256 matrix and short TE (3.3msec or less) seems feasible at 3T.

2. Introduction

Coil placement has been proven to be safe and effective in the treatment of intracranial aneurysms (43, 44). However, several previous studies have also reported that patients treated with platinum coils can have a recurrence at the aneurysm neck, even in cases of initial total occlusion

(45, 46). Therefore, long-term follow-up with neuroimaging is necessary to establish the stability of endovascular treatment and to depict a recanalization that may require further treatment. Three-dimensional time-of-flight (3D TOF) magnetic resonance angiography (MRA) is now readily accepted as a noninvasive imaging modality, which may be comparable to digital subtraction angiography (DSA) to assess aneurysm remnants and parent vessel stenosis after aneurysm coiling (13, 14, 47).

With regard to 3D TOF MRA, the 3T system offers some potential advantages compared to a 1.5T system. The approximate doubling of the signal-to-noise ratio (SNR) from 1.5 to 3T can provide higher spatial resolution (33, 34) and the increased T1 relaxation time at higher magnetic field strength yields improvement of vessel–tissue contrast at 3T imaging (28). Therefore, these advantages provide prospects for further improvement of depiction of aneurysm remnants. On the other hand, one of the major limitations of 3T MRA is its greater susceptibility effects, which can increase the varying degrees of susceptibility-induced artifact created by platinum coils. A previous study using an aneurysm phantom has reported that the imaging at 3T does not provide an incremental gain for 3D TOF sequences compared to that at 1.5T because of significant increases in coil-induced artifacts (48). The authors, however, were not able to determine the overall image quality of the 3D TOF MRA because they used a closed aneurysm phantom with no flow, which cannot estimate the effects of flowing blood within the aneurysm. Majoie et al (49) reported that high-spatial-resolution

3D TOF MRA at 3T is feasible and useful in the follow up of patients with intracranial aneurysms treated with coil placement and the susceptibility-induced artifact created by platinum coils were minimal; however, they did not compare 3D TOF sequences between 1.5T and 3T.

The purpose of this study was to analyze the influence of the matrix and the echo time (TE) of 3D TOF MRA on the depiction of residual flow in aneurysms embolized with platinum coils at 1.5T and 3T and to establish the optimal parameters using a vascular phantom with a pulsatile flow.

3. MATERIALS AND METHODS

Phantom Design and Embolization of Simulated Aneurysms

An anthropomorphic vascular phantom (Renaissance of Technology, Shizuoka, Japan) consisted of a 19cm-diameter cylinder made of silicone rubber was designed to simulate the bilateral intracranial arteries

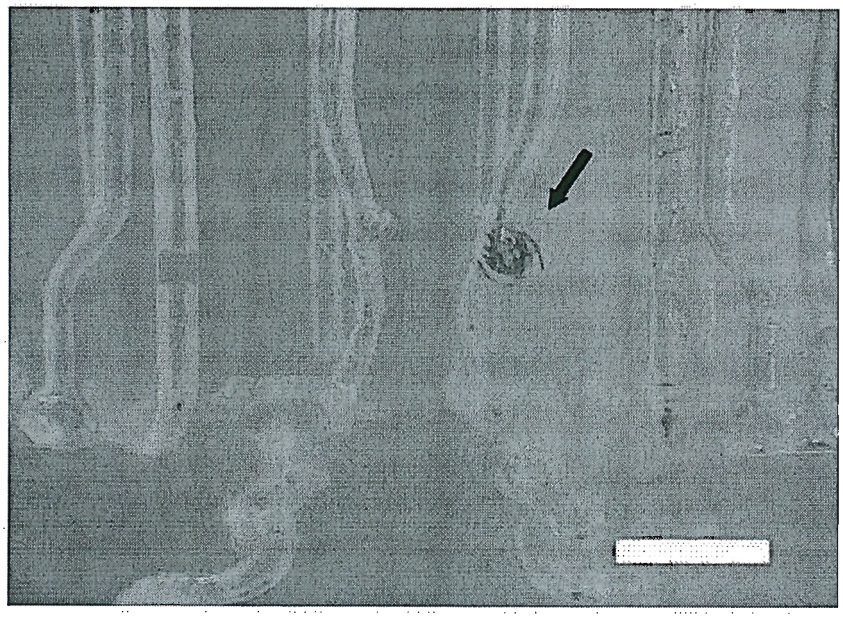

Figure 1. Photograph shows an aneurysm in the phantom (arrow) packed to maintain patency of some residual aneurysmal lumen with the interlocking detachable coils.

with various intracranial aneurysms. One of the simulated aneurysms with diameter of 6 mm was loosely packed to maintain patency of some residual aneurysmal lumen with the interlocking detachable coils (IDCs; Boston Scientific/Target Therapeutics, Watertown, MA) (Fig. 1). The other aneurysms were not packed with IDC. A tracker catheter (Target Therapeutics/ Boston Scientific) was introduced into the aneurysm and IDCs were positioned in the dome of the simulated aneurysm, and the aneurysm model with IDCs was constructed.

The embolized volume was calculated using the following equation: embolized volume =(volume of the embolized coil) / (volume of the aneurysm). The volume of the coil is approximately calculated based on the supposition that the coil is a cylinder. The algebraic equation to calculate the volume of the coil is: volume of coil = πx (diameter of coil / 2)^2 × length of coil. The primary diameter of each type of coil is published by Boston Scientific, Target (Fremont, CA). Assuming an aneurysm model of 6 × 6 × 4 mm3, the aneurysm volume was also calculated by using the following formula: volume of the aneurysm =4π/3 ×(width/2) × (length/2) × (height/2) mm3. Therefore, the aneurysm model with IDC achieved the embolized volume: 6 × 6 × 4 mm^3, 29.8% occlusion.

Image Acquisition

The phantom tube filled with gadodiamide-saline solution was connected to an electromagnetic flow pump (LMI Milton Roy, Acton, MA) that allowed

pulsatile perfusion with pulse rates between 40 and 100 beats per minute. To emulate the flow characteristics of blood, the T1 of the solution obtained at 1.5T was adjusted to 900 msec with gadopentetate dimeglumine (37). The phantom was connected to a system of reservoirs and a pump that maintained a constant pressure difference across the flow tube within the phantom. The pulsatile flow was generated by a pulsatile blood pump (model 1405; Harvard Apparatus, Ealing; South Natick, MA). In this pump an electric motor drives a flywheel, which pushes a plunger in and out of a cylinder. As the plunger moves forward, flow is ejected out of the oneway valve and is propelled toward the flow circuit. Pulsatile flow with a pulsation rate of 50 pulses per minute and mean velocity of 25 cm/sec (maximum; 50 cm/sec) was produced in the experimental assembly in a closed system.

MRA studies were performed with a Signa EXCITE 1.5T MR system (GE Medical Systems, Milwaukee, WI) and a Signa EXCITE 3T MR system (GE Medical Systems) by using a dedicated eight-channel phased-array coil (USA Instruments, Aurora, OH). For the aneurysm with IDCs, various 3D TOF sequences were performed at 1.5T and 3T MRI systems (Table 1). Variables included the TE, acquired voxel dimension, and acquisition time. For all 3D TOF sequences, the following parameters were kept constant: repetition time (TR = 30 msec), bandwidth (BW = 65 kHz), field of view (FOV = 18 cm), flip angle (FA = 20°), section thickness (ST = 1.0 mm), and phase encoding direction. Therefore, for the 1.5T and 3T systems a total of 22 MR angiograms were prepared in this study.

Table 1
Scanning Parameters for the 3D Time-of-Flight MR Angiography and the Results of Subjective Evaluation

Sequence No.	TE	F-E mtx	SENSE RF	NEX	AT	Effect on parent artery	Depiction of aneurysm remnant
1.5T							
1	6.5	256 × 160	NA	2 times	9 min 18 sec	major	not visible
2	3.3	256 × 160	NA	2 times	9 min 18 sec	minor	adequate
3	6.5	256 × 160	1.3	1 time	4 min 44 sec	major	not visible
4	4.5	256 × 160	1.3	1 time	4 min 44 sec	moderate	inadequate
5	3.3	256 × 160	1.3	1 time	4 min 44 sec	minor	inadequate
6	2.8	256 × 160	1.3	1 time	4 min 44 sec	minor	adequate
7	6.5	384 × 224	1.3	1 time	6 min 36 sec	major	not visible
8	4.5	384 × 224	1.3	1 time	6 min 36 sec	moderate	not visible
9	3.3	384 × 224	1.3	1 time	6 min 36 sec	minor	inadequate
10	2.8	384 × 224	1.3	1 time	6 min 36 sec	minor	inadequate
3T							
1	6.5	256 × 160	2.0	1 time	3 min 10 sec	major	not visible
2	4.5	256 × 160	2.0	1 time	3 min 10 sec	major	not visible
3	3.3	256 × 160	2.0	1 time	3 min 10 sec	moderate	inadequate
4	2.8	256 × 160	2.0	1 time	3 min 10 sec	minor	adequate
5	1.7	256 × 160	2.0	1 time	3 min 10 sec	minor	adequate
6	6.5	384 × 224	2.0	1 time	4 min 25 sec	major	not visible
7	4.5	384 × 224	2.0	1 time	4 min 25 sec	moderate	adequate
8	3.3	384 × 224	2.0	1 time	4 min 25 sec	minor	good
9	2.8	384 × 224	2.0	1 time	4 min 25 sec	minor	excellent
10	1.7	384 × 224	2.0	1 time	4 min 25 sec	minor	excellent
11	3.3	512 × 256	2.0	1 time	5 min 2 sec	minor	excellent
12	1.7	512 × 256	2.0	1 time	5 min 2 sec	minor	excellent

Note.—TE, echo time; F-E mtx, frequency-encoded matrix; SENSE RF, SENSE reduction factor; NEX, number of excitation; AT, acquisition time; NA, not applicable

Image Analysis of MRA

The image quality of the MRA obtained with the 1.5T and 3T systems was evaluated together by two neuroradiologists (N.O., J.M.) according to the following criteria: the depiction of aneurysm remnants and the degree of coil-induced artifacts and the final judgments were obtained by consensus. For interpretation of the MRA, these radiologists were blinded to the MR imaging systems (1.5T and 3T systems) and MR imaging parameters (TE, voxel dimension, acquisition time, etc). Before the evaluations these radiologists were informed of the packing percentage. The schematic drawing of an anthropomorphic vascular phantom and the aneurysm after the insertion of IDCs were always used as the standard of reference (Fig. 1). MR angiographic source and maximum intensity

Table 2
Image Scores of MRA

Depiction of aneurysm remnants
excellent = aneurysm remnants were clearly visualized
good = aneurysm remnants were satisfactory visualized but the signal intensity in a patent lumen of aneurysm somewhat reduced
adequate = visualization of aneurysm remnants were still sufficient for
inadequate = insufficient visualization and difficult to diagnose with confidence not visible
Coil-induced artifacts
none = artifact has no influence on the depiction of a parent artery
minor = artifact causes minor pseudostenosis of a parent artery
moderate = artifact causes the marked pseudostenosis of parent artery sufficient to interfere with diagnostic quality
major = artifact results in a nondiagnostic study

projection (MIP) images were used for this evaluation. A five-grade system was used to evaluate the depiction of aneurysm remnants (Table 2). These radiologists also evaluated whether the coil-induced artifacts affected the depiction of a parent artery. The effects of the coil-induced artifacts on the depiction of a parent artery were judged by using a four-grade system (Table 2). In assessing the MR angiograms, each image was analyzed separately and only one image was shown at a time. The MR angiograms were displayed and interpreted on a diagnostic monitor (Flexscan L365; Eizo Nanao, Ishikawa, Japan). An intuitive and efficient user interface allows the manipulation (eg, rotation, zoom, electronic scalpel) of these views in real time, and the reviewers determined the threshold of vessel images in each subject by interactively observing the angiograms at the workstation.

4. RESULTS

The results of the final consensus reviewed by two radiologists on the image quality of 1.5T and 3T MRA are summarized in Table 1.

At 3T the depiction of the aneurysm remnant was gradually

superior as matrix size increased. With a TE of 3.3 msec at 3T the depiction of an aneurysm remnant was scored as "good" with a matrix size of 384 × 224 and "excellent" with a matrix size of 512 × 256, whereas it was scored as "inadequate" with a matrix size of 256 _ 160. In contrast, the aneurysm remnant was not sufficiently visualized on 1.5T MRA with a matrix size of 384 × 224 with any TEs.

At 3T the depiction of the aneurysm remnant improved as the TE was reduced. For example, with a matrix size of 384 × 224 at 3T the radiologists scored the depiction of an aneurysm remnant as "not visible" on MRA with a TE of 6.5 msec, "adequate" with a TE of 4.5 msec, "good" with a TE of 3.3 msec, and "excellent" with TEs of 2.8 msec and 1.7 msec (Fig. 2). With a TE of 3.3 msec at 3T the depiction of an aneurysm remnant was scored as "good" with a matrix size of 384 × 224 and "excellent" with a matrix size of 512 × 256; however, it was scored as "inadequate" with a matrix size of 256 × 160 (Fig. 3).

For the depiction of an aneurysm remnant, the high-spatial-resolution 3T MRA (matrix size of 384 × 224 and 512 × 256) with a short TE of ≦ 3.3 msec was superior to the 1.5 T MRA obtained with any sequences. For example, for a short TE of ≦3.3 msec the high-spatial- resolution 3T MRA with an acquisition time of 4minutes 25 seconds was superior to 1.5T MRA with an acquisition time of 9 minutes 18 seconds for the depiction of an aneurysm remnant. For both 1.5T and 3T MRA with a TE of 6.5 msec the effect of coil-induced artifact on the

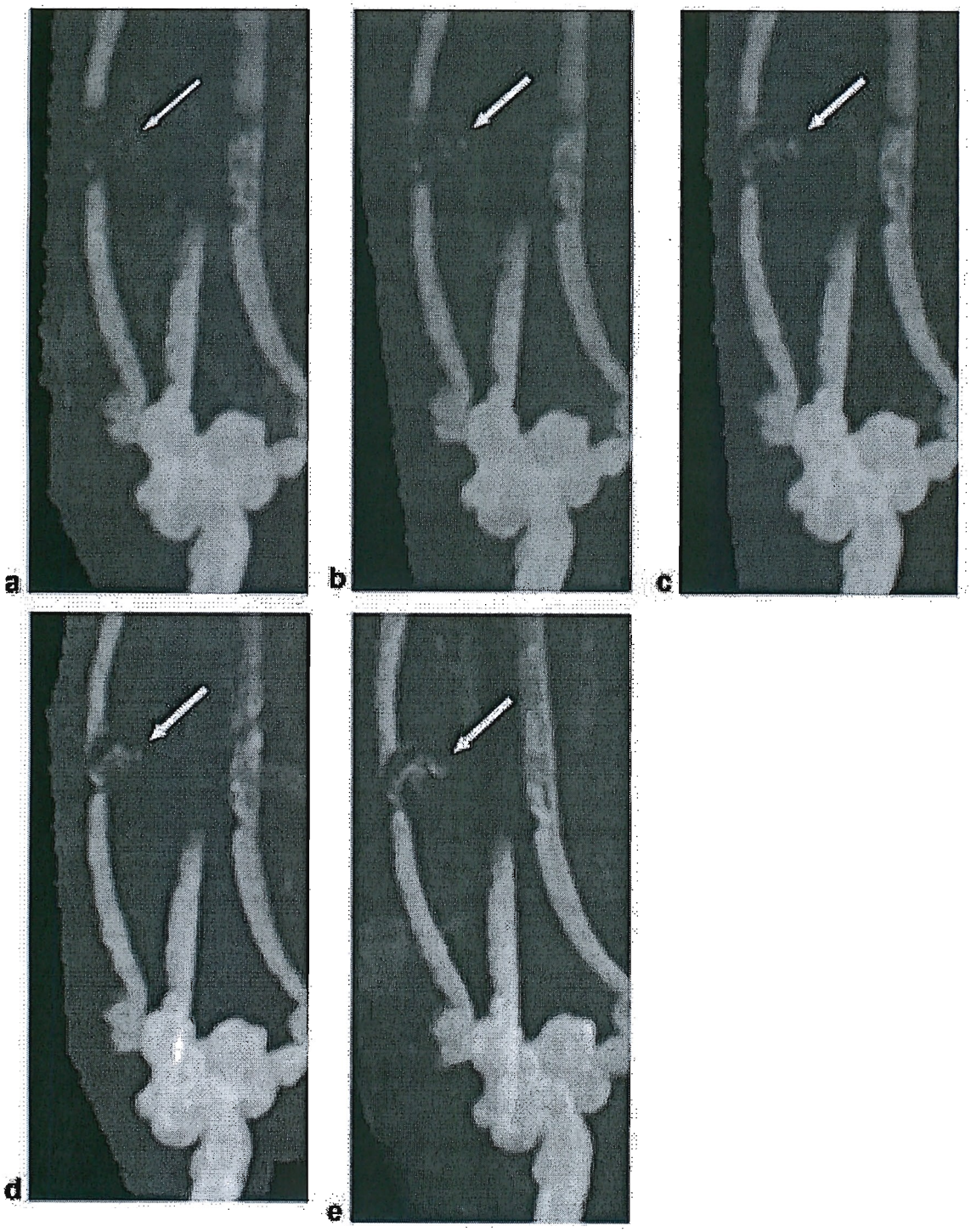

Figure 2. a–j: 3D TOF MRA of the simulated aneurysm embolized with platinum coils (29.8% occlusion) obtained with various TEs at 3T (matrix size of 384 × 224): MIP and source images with the TE of 6.5 msec (a,f), 4.5 msec (b,g), TE of 3.3 msec (c,h), TE of 2.6 msec (d,i), and TE of 1.7 msec (e,j). The white arrows in the MIP images indicate the aneurysm remnant. The dotted circles in the source images indicate the margin of the aneurysm. The shorter the TE, the better the depiction of the aneurysm remnant. The TE of 3.3 msec or shorter is necessary for the depiction of the aneurysm remnant.

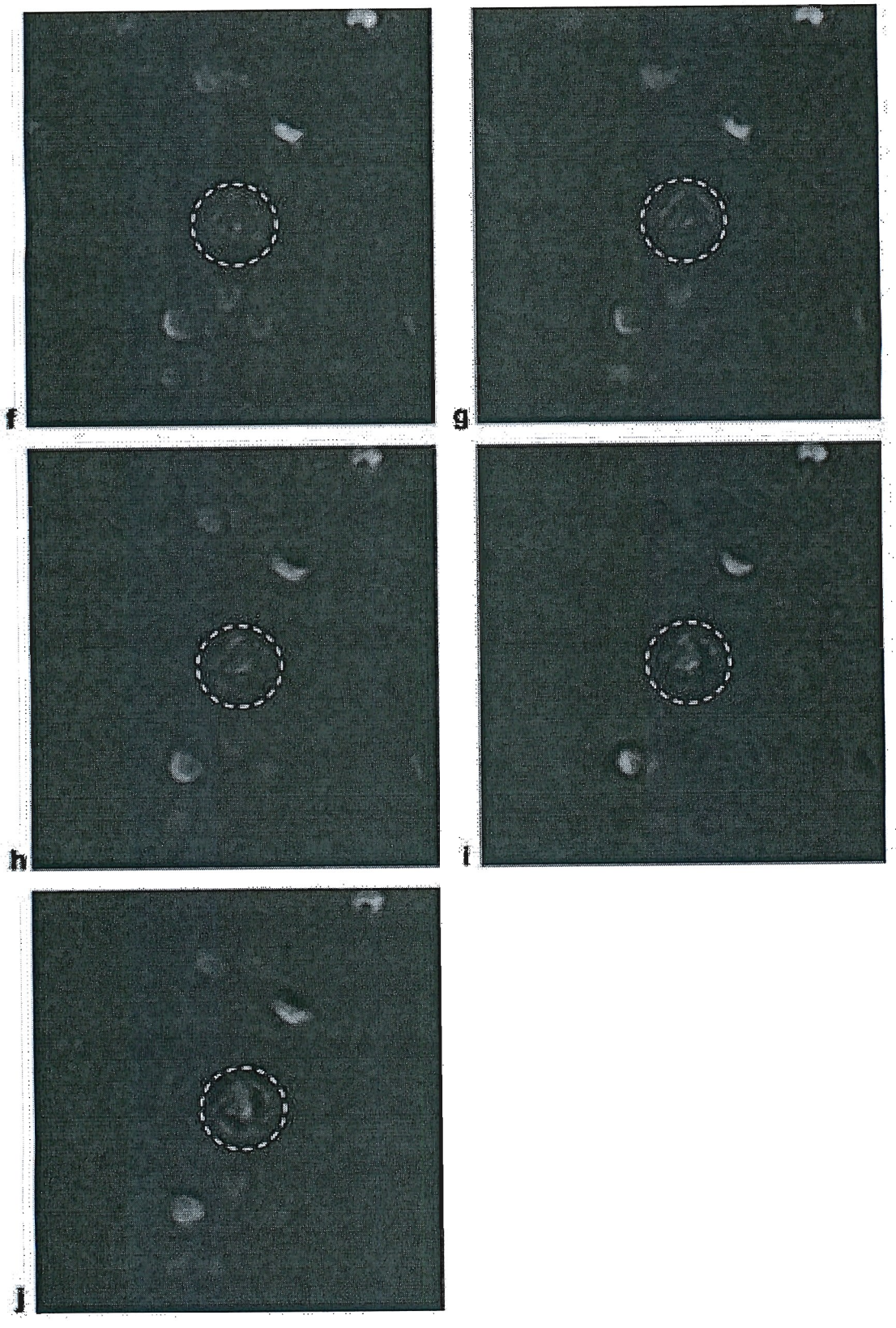

Figure 2 (Continued)

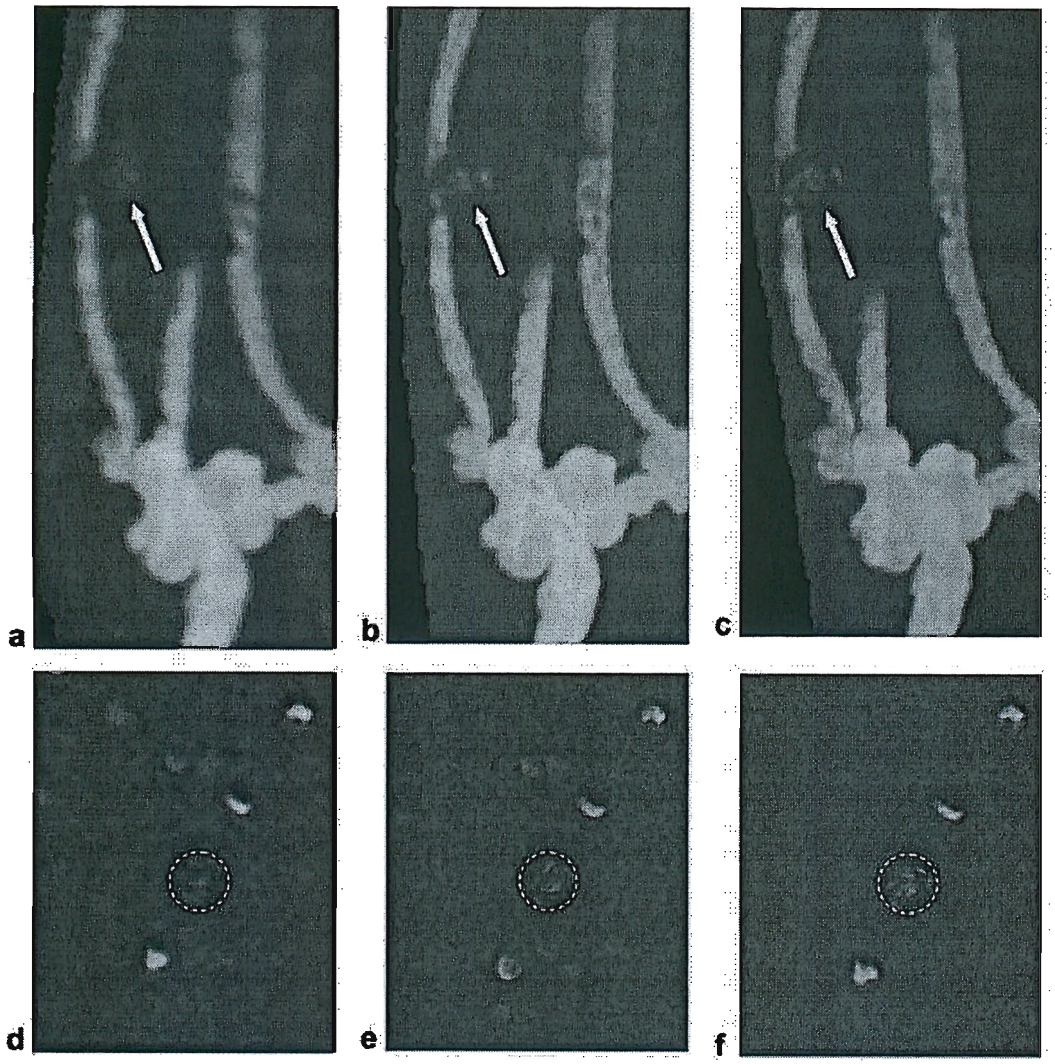

Figure 3. a–f: 3D TOF MRA of the simulated aneurysm embolized with platinum coils (29.8% occlusion) obtained with various matrix sizes at 3T (TE 3.3 msec): MIP and source images with a matrix size of 256 × 160 (a,d), 384 224 (b,e), and 512 × 256 (c,f). The white arrows in the MIP images indicate the aneurysm remnant. The dotted circles in the source images indicate the margin of the aneurysm. The aneurysm remnant is sufficiently depicted with a matrix size of 384 × 224 or 512 × 256, whereas a matrix size of 256 × 160 is insufficient (inadequate visualization).

depiction of a parent artery was scored "major." When a 3D TOF sequence with the short TE of ≦ 3.3 msec was used there was no definite difference between both field strengths with regard to the effects of the coil-induced artifacts on the depiction of a parent artery.

DISCUSSION

For comparison of MRA obtained with the same TE, the high-spatial-resolution 3T MRA (2 ⊃ m) was superior to any 1.5T or the standard 3T MRA with a matrix size of 256 × 160 in the depiction of the aneurysm remnant. With the improved SNR at 3T it is possible to increase the spatial resolution at 3D TOF MRA with preservation of image quality (33, 34). On the other hand, the results indicated that further increases in spatial resolution at 1.5T MRA could not improve the depiction of the aneurysm remnant. Further increases in the spatial resolution at 1.5T imaging caused further reduction of SNR and would simultaneously degrade image quality. Therefore, the spatial resolution at 3D TOF MRA is still limited at 1.5T.

For the depiction of the aneurysm remnant, the high-spatial-resolution 3T MRA with an acquisition time of 4 minutes 25 seconds using a reduction factor 2 was superior to the 1.5T MRA with an acquisition time of 9 minutes 18 seconds. A parallel imaging technique such as sensitivity encoding (SENSE) has been proposed to markedly reduce image acquisition time (40–42). The high-spatial-resolution 3T MRA may certainly benefit from the use of a parallel imaging technique to reduce the acquisition time while maintaining the high spatial resolution. On the other hand, a decrease in the SNR inherent to SENSE has been reported (41); the reduction in SNR is characterized by the square root of the reduction factor. Although we used a 1.3 reduction factor at 1.5T, which was smaller than 2.0 at 3T, the parallel imaging technique may have still affected the image

quality of 1.5T MRA because the image degradation caused by the parallel imaging technique seems to be more prominent at 1.5T than at 3T.

Any material whose static magnetic susceptibility differs from that of surrounding tissues will distort the magnetic (B0) field. In addition, dynamic eddy currents in the conduction of materials caused by time variable magnetic fields, such as radiofrequency (RF) and B0 gradient fields, may lead to B1 field homogeneity, image intensity, and distortion artifacts (24). These effects with metal also cause the image degradation in 3D TOF MRA, which is the limiting factor in the assessment of aneurysm remnants and parent vessel stenosis after aneurysm coiling (50). Previous studies have reported that reducing the TE reduced the heterogeneity of the magnetic field that occurs with metal (48, 51, 52). Gonner et al (51) reported that the MR angiographic technique with a short TE of 2.4 could depict more diagnostically relevant adjacent vessels by reducing the extent of coil-induced artifacts. Regarding the 3D TOF sequence at 3T, Walker et al (48) reported that reducing the TE from 7.2 msec to 3.5 msec was effective for minimizing coil-induced artifacts. Similar to previous assertions, our results of MRA at 3T showed that the depiction of the aneurysm remnant was gradually superior as the TE was reduced, which is consistent with the findings of previous studies. Some studies have reported that the coil-induced signal intensity loss mimicked a narrowing or occlusion of the parent and branch vessels on MR angiograms (14, 53). In this study there was no definite difference between both field strengths regarding the effects of the coil-induced artifacts on the depiction

of a parent artery when a 3D TOF sequence with a short TE of smaller reductions below 3.3 msec was used. The echo delay of 1.1 msec, 3.3 msec, and 5.5 msec places lipids and water out of phase at 3T, which leads to low signal on gradient echoes in all voxels that contain water and lipid components. Therefore, the combination of the matrix of 512 × 256 and the TE of 3.3 or 1.1 msec may be optimal at 3T when considering acquisition time and opposed phase of TE.

There are a few limitations in this study. First, the anthropomorphic vascular phantom was made of silicone rubber. In 3D TOF MRA, diminution of signal intensity loss due to spin dephasing is resolved most effectively with implementation of short TE (52). Coincidentally, the sequence with shorter TE may cause a reduction of vascular contrast because of a higher signal from the background tissue. MRA at a higher field strength results in a more efficient suppression of the background tissue because the T1 longitudinal relaxation time is longer (28, 34), providing an improvement of vascular contrast. In this study it was impossible to know whether these factors associated with the phantom made of silicone rubber would tend to overestimate or underestimate the image quality of MRA at 3T compared with human MR examination. Second, since an MRA cannot depict the coils themselves, the coil compaction was estimated by using an actual simulated aneurysm after the insertion of IDCs as the standard of reference. However, it was not possible to precisely determine whether a localized signal intensity loss in the parent artery was due to coil-induced artifacts or turbulence induced by protrusion

of the coils. In this study a simulated aneurysm with a diameter of 6 mm was loosely packed with the IDCs, which were relatively small objects less affected by coil-induced artifacts. Despite these limitations, it is important to compare two systems under the same experimental conditions. Third, we did not evaluate DSA imaging of the phantom, although DSA is always used for a rough evaluation of an aneurysm remnant during embolization with platinum coils in a clinical situation. The embolized ratio calculated from the aneurysmal volume and theoretical coil volume, which we adopted in this study, is also considered an important standard when assessing whether coil embolization is sufficient or not. The previous study reported that the probability of coil compaction was significantly higher when the coil-packing ratio was less than 50% (54). Fourth, we did not use the contrast-enhanced MRA technique in our phantom study. Although some authors have reported that the contrast-enhanced MRA at 1.5T constitutes a reliable technique for the detection of aneurysm remnants (55, 56), the optimal protocol for contrast-enhanced MRA at 3T has not been fully evaluated. Therefore, further investigation with regard to the contrast-enhanced MRA at 3T is necessary.

In an attempt to establish the optimal parameters at 3T, 3D TOF MRA at 3T was compared with that at 1.5T to assess the depiction of residual flow in an aneurysm embolized with platinum coils by using a vascular phantom with pulsatile flow. In conclusion, the high-spatial-resolution MRA at 3T with short TE of $\leqq$ 3.3 msec offers superior image quality for the depiction of aneurysm remnants compared

with 1.5T. Among the 3T MRAs obtained with TE ≦ 3.3 msec, the best image quality regarding the depiction of the aneurysm remnant was obtained with a matrix size of 512 × 256.

References

1. Bosmans H, Marchal G, Lukito G, Yicheng N, Wilms G, Laub G, Baert AL. Time-of-flight MR angiography of the brain: comparison of acquisition techniques in healthy volunteers. Am J Roentgenol 1995; 164:161–167
2. Dumoulin CL, Souza SP, Walker MF, Wagle W. Three-dimensional phase contrast angiography. Magn Reson Med 1989; 9:139–149
3. Marks MP, Pelc MJ, Ross MR, Enzmann DR. Determination of cerebral blood flow with a phase-contrast cine MR imaging technique: evaluation of normal subjects and patients with arteriovenous malformation. Radiology 1992; 182:467–476
4. Hausmann R, Lewin JS, Laub G. Phase-contrast MR angiography with reduced acquisition time: new concepts in sequence design. J Magn Reson Imaging 1991; 1:415–422.
5. Riederer SJ, Bernstein MA, Breen JF, Busse RF, Ehman RI, Fain SB, Hulshizer TC, Iii JH, King BF, Kruger DG, Rosmann PJ, Shah S. Three dimensional contrast-enhanced MR angiography with real-time fluoroscopic triggering: design specifications and technical reliability in 330 patient studies. Radiology 2000; 215:584–593
6. Heiserman JE, Dean BL, Hodak JA, Flom RA, Bird CR, Drayer BP, Fram EK. Neurological complications of cerebral angiography. Am J Neuroradiol 1994; 15:1401–1407
7. Sankhla SK, Gunawardena WJ, Coutinho CMA, Jones AP, Keogh AJ.

Magnetic resonance angiography in the management of aneurysmal subarachnoid hemorrhage: a study of 51 cases. Neuroradiology 1996; 38:724–729

8. Bosmans H, Wilms G, Marchal G,Demaerel P, Baert AL. Characterization of intracranial aneurysms with MR angiography. Neuroradiology 1995; 37:262–266
9. Adams WM, Laitt RD, Jackson A. The role of MR angiography in the pretreatment assessment of intracranial aneurysms: a comparative study. Am J Neuroradiol 2000; 21:1618–1628
10. White PM, Wardlaw JM, Lindsay KW, Sloss S, Patel DK, Teasdale EM. The non-invasive detection of intracranial aneurysms: are neuroradiologists any better than other observers? Eur Radiol 2003; 13:389–396
11. Fernandez-Zubillaga A, Guglielmi G, Vinuela F, Duckwiler G. Endovascular occlusion of intracranial aneurysms with electrolytically detachable coils: correlation of aneurysm neck size and treatment results. Am J Neuroradiol 1994; 15:815–820
12. Cottier JP, Bleuzen-Couthon A, Gallas S, Vinikoff-sonier CB, Bertrand P, Domengie F, Barantin L, Herbreteau D. Intracranial aneurysms treated with Guglielmi detachable coils: is contrast material necessary in the follow-up with 3D time-of-flight MR angiography? Am J Neuroradiol 2003; 24:1797–1803
13. Kahara VJ, Seppanen SK, Ryymin PS, Mattila P, Kuurne T, Laasonen EM . MR angiography with threedimensional time-of-flight and

targeted maximum-intensity-projection reconstructions in the follow-up of intracranial aneurysms embolized with Guglielmi detachable coils. Am J Neuroradiol 1999; 20:1470–1475

14. Anzalone N, Righi C, Simionato F, Scomazzoni F, Pagani G, Calori G, Santino P, Scotti G. Threedimensional time-of-flight MR angiography in the evaluation of intracranial aneurysms treated with Guglielmi detachable coils. Am J Neuroradiol 2000; 21:746–752
15. Boulin A, Pierot L. Follow-up intracranial aneurysms treated with detachable coils: comparison of gadolinium enhanced 3D time-of-flight MR angiography and digital subtraction angiography. Radiology 2001; 219:108–113
16. Haacke EM, Lenz GW. Improving MR image quality in the presence of motion by using rephasing gradients. Am J Radiol 1987; 148: 1251–1258.
17. Laub G, Kaiser WA. MR angiography with gradient motion refocusing. J Comput Assist Tomogr 1988; 12: 377–382.
18. Blatter DD, Parker DL, Ah SS, Bahr AL, Robinson RO, Schwartz RB, Jolesz FA, Boyer RS. Cerebral MR angiography with multiple overlapping thin slab acquisition. Part II. Early clinical experience. Radiology 1992; 183: 379–389
19. Mathews VP, Elster AD, King JC, Ulmer JL, Hamilton CA, Strottmann JM. Combined effects of magnetization transfer and gadolinium in cranial MR imaging and MR angiography. Am J Roentgenol 1995; 164:169–172

20. Haacke EM, Masaryk TJ, Wielopolski PA, Zypman FR, Tkach JA, Amartur S, Mitchell J, Clampitt M, Paschal C. Optimizing blood vessel contrast in fast three-dimensional MRI. Magn Reson Med 1990; 14:202–221
21. Atkinson D, Brandt-Zawadzki M, Gillan G, Purdy D, Laub G. Improved MR angiography magnetization transfer suppression with variable flip angle excitation and increased resolution. Radiology 1994; 190: 890–894
22. Marchal G, Michiels J, Bosmans H, Van Hecke P. Contrast enhanced MRA of the brain. J Comput Assist Tomogr 1992; 16:25–29
23. Wilms G, Bosmans H, Demaerel Ph, Marchal G. Magnetic resonance angiography of the intracranial vessels. Eur J Radiol 2001; 38:10–18
24. Camacho CR, Plewes DB, Henkelman RM. Nonsusceptibility artifacts due to metallic objects in MR imaging. J Magn Reson Imaging 1995; 5: 75–88.
25. Wilcock DJ, Jaspan T, Worthington BS. Problems and pitfalls of 3-D TOF magnetic resonance angiography of the intracranial circulation. Clin Radiol 1995; 50: 526–532.
26. Willinek WA, Born M, Simon B, et al. Time-of-flight MR angiography: comparison of 3.0-T imaging and 1.5-T imaging—initial experience. Radiology 2003; 229: 913–920.
27. Gibbs GF, Huston J III, Bernstein MA, Riederer SJ, Brown RD. Improved image quality of intracranial aneurysms: 3T versus 1.5-T time-of-flight MR angiography. AJNR Am J Neuroradiol 2004; 25:

84–87.

28. Al-Kwifi O, Emery DJ, Wilman AH. Vessel contrast at three Tesla in time-of-flight magnetic resonance angiography of the intracranial and carotid arteries. Magn Reson Imaging 2002; 20: 181–187.
29. Korogi Y, Takahashi M, Mabuchi N, et al. Intracranial aneurysms: diagnostic accuracy of three-dimensional, Fourier transform, time-of-flight MR angiography. Radiology 1994; 193:187-193.
30. White PM, Teasdale EM, Wardlaw JM, Easton V. Intracranial aneurysms: CT angiography and MR angiography for detection prospective blinded comparison in a large patient cohort. Radiology 2001; 219:739-749.
31. Huston J III, Nichols DA, Luetmer PH, et al. Blinded prospective evaluation of sensitivity of MR angiography to known intracranial aneurysms: importance of aneurysm size. AJNR Am J Neuroradiol 1994; 15:1607-1614.
32. Fujita N, Hirabuki N, Fujii K, Hashimoto T, Miura T, Sato T, Kozuka T. MR imaging of middle cerebral artery stenosis and occlusion: value of MR angiography.AJNR Am J Neuroradiol. 1994 ;15(2):335-341. Erratum in: AJNR Am J Neuroradiol 1994; 15:9-10.
33. Willinek WA, Born M, Simon B, Tschampa HJ, Krautmacher C, Gieseke J, Urbach H, Textor HJ, Schild HH. Time-of-flight MR angiography: comparison of 3.0-T imaging and 1.5-T imaging--initial experience. Radiology. 2003; 229: 913-920
34. Gibbs GF, Huston J III, Bernstein MA, Riederer SJ, Brown RD.

Improved image quality of intracranial aneurysms: 3T versus 1.5-T time-of-flight MR angiography. AJNR Am J Neuroradiol 2004; 25: 84–87

35. Fushimi Y, Miki Y, Kikuta K, Okada T, Kanagaki M, Yamamoto A, Nozaki K, Hashimoto N, Hanakawa T, Fukuyama H, Togashi K. Comparison of 3.0- and 1.5-T three-dimensional time-of-flight MR angiography in moyamoya disease: preliminary experience. Radiology 2006 ; 239: 232-237.
36. Gaa J, Weidauer S, Requardt M, Kiefer B, Lanfermann H, Zanella FE. Comparison of intracranial 3D-ToF-MRA with and without parallel acquisition techniques at 1.5T and 3.0T: preliminary results. Acta Radiol. 2004 May; 45: 327-32
37. Wolf RL, Richardson DB, LaPlante CC, Huston J 3rd, Riederer SJ, Ehman RL. Blood flow imaging through detection of temporal variations in magnetization. Radiology 1992; 185: 559-567.
38. Sodickson DK, Manning WJ. Simultaneous acquisition of spatial harmonics (SMASH): fast imaging with radiofrequency coil arrays. Magn Reson Med 1997; 38: 591-603.
39. Pruessmann KP, Weiger M, Scheidegger MB, Boesiger P. SENSE: sensitivity encoding for fast MRI. Magn Reson Med 1999; 42: 952-962.
40. Griswold MA, Jakob PM, Nittka M, Goldfarb JW, Haase A. Partially parallel imaging with localized sensitivities (PILS). Magn Reson Med 2000; 44: 602-609.
41. Weiger M, Pruessmann KP, Leussler C, Roschmann P, Boesiger P.

Specific coil design for SENSE: a six-element cardiac array. Magn Reson Med 2001; 45:495-504.

42. Weiger M, Pruessmann KP, Kassner A, et al. Contrast-enhanced 3D MRA using SENSE. J Magn Reson Imaging 2000; 12: 671-677.
43. Molyneux A, Kerr R, Stratton I, et al. International Subarachnoid Aneurysm Trial (ISAT) Collaborative Group. International Subarachnoid Aneurysm Trial (ISAT) of neurosurgical clipping versus endovascular coiling in 2143 patients with ruptured intracranial aneurysms: a randomised trial. Lancet 2002; 360: 1267–1274.
44. Brilstra EH, Rinkel GJ, van der Graaf Y, van Rooij WJ, Algra A. Treatment of intracranial aneurysms by embolization with coils: a systematic review. Stroke 1999; 30: 470–476.
45. Cognard C, Weill A, Castaings L, et al. Intracranial berry aneurysms: angiographic and clinical results after endovascular treatment. Radiology 1998; 206: 499–510.
46. Cognard C, Weill A, Spelle L, et al. Long-term angiographic follow-up of 169 intracranial berry aneurysms occluded with detachable coils. Radiology 1999; 212: 348–356.
47. Derdeyn CP, Graves VB, Turski PA, et al. MR angiography of saccular aneurysms after treatment with Guglielmi coils: preliminary experience. AJNR Am J Neuroradiol 1997; 18: 279–286.
48. Walker MT, Tsai J, Parish T, et al. MR angiographic evaluation of platinum coil packs at 1.5T and 3T: an in vitro assessment of artifact production: technical note. AJNR Am J Neuroradiol 2005; 26:

848–853.

49. Majoie CB, Sprengers ME, van Rooij WJ, et al. MR angiography at 3T versus digital subtraction angiography in the follow-up of intracranial aneurysms treated with detachable coils. AJNR Am J Neuroradiol 2005; 26: 1349–1356.
50. Wilcock DJ, Jaspan T, Worthington BS. Problems and pitfalls of 3-D TOF magnetic resonance angiography of the intracranial circulation. Clin Radiol 1995; 50: 526–532.
51. Gonner F, Heid O, Remonda L, et al. MR angiography with ultrashort echo time in cerebral aneurysms treated with Guglielmi detachable coils. AJNR Am J Neuroradiol 1998; 19: 1324–1328.
52. Schmalbrock P, Yaun C, Chakeres DW, et al. MR angiography: methods to achieve very short echo times. Radiology 1990; 175: 861–865.
53. Brunereau L, Cottier JP, Sonier CB, et al. Prospective evaluation of time-of-flight MR angiography in the follow-up of intracranial saccular aneurysms treated with Guglielmi detachable coils. J Comput Assist Tomogr 1999; 23: 216–223.
54. Kai Y, Hamada J, Morioka M, Yano S, Kuratsu J. Evaluation of the stability of small ruptured aneurysms with a small neck after embolization with Guglielmi detachable coils: correlation between coil packing ratio and coil compaction. Neurosurgery 2005; 56: 785– 792.
55. Gauvrit JY, Leclerc X, Pernodet M, et al. Intracranial aneurysms treated with Guglielmi detachable coils: usefulness of 6-month imaging

follow-up with contrast-enhanced MR angiography. AJNR Am J Neuroradiol 2005; 26: 515–521.

56. Leclerc X, Navez JF, Gauvrit JY, Lejeune JP, Pruvo JP. Aneurysms of the anterior communicating artery treated with Guglielmi detachable coils: follow-up with contrast-enhanced MR angiography. AJNR Am J Neuroradiol 2002; 23: 1121–1127.